A Draft LANL-Local Tech Note

on the Forward sPHENIX Upgrade

(The "short' version as of November 25, 2013.)

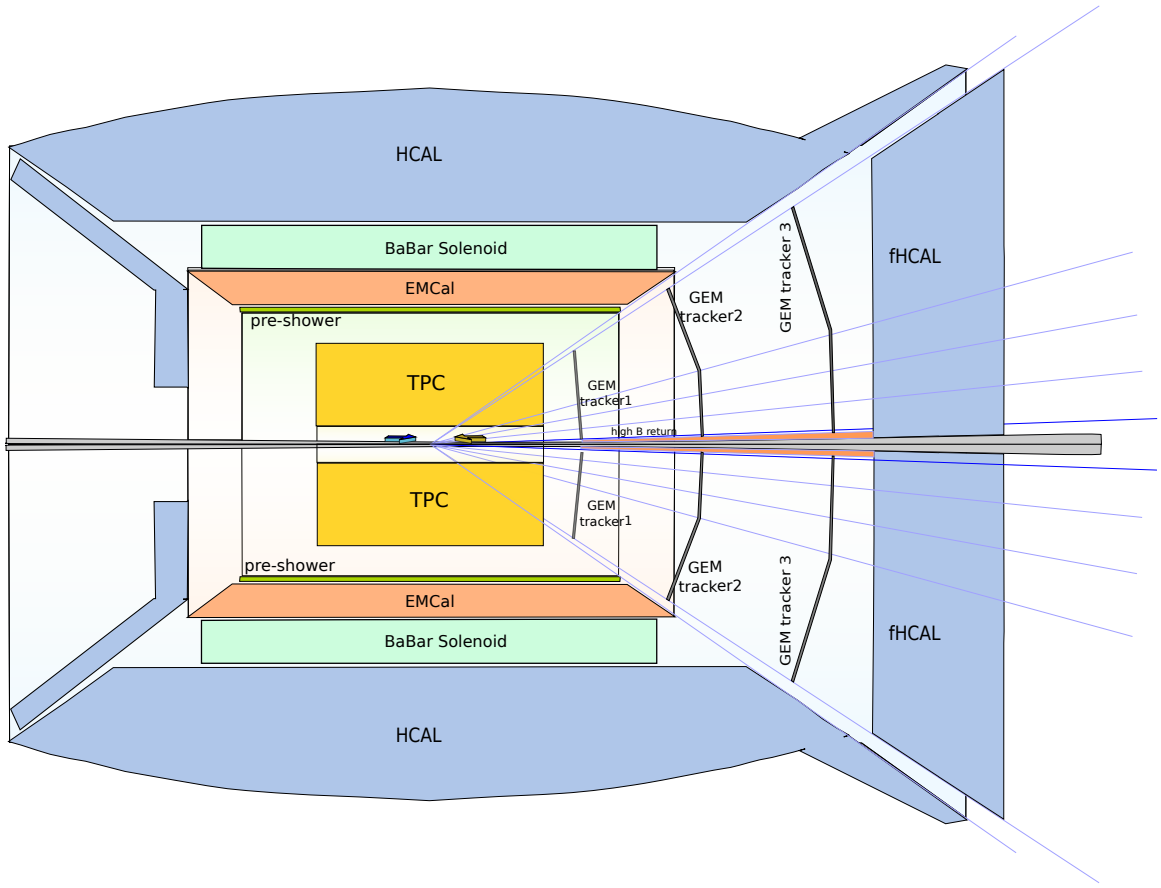

LANL folks + other collaborators later BNL, RIKEN etc.

Melynda Brooks, Hubert van Hecke, Matt Durham, Jin Huang, Xiaodong Jiang, Zhongbo Kang, Kwangbok Lee, Mike Leitch, Kun Liu, Ming X. Liu, Mike McCumber, Patrick McGaughey, Cesar Luiz da Silva
Los Alamos National Laboratory

This is the "short" version of the fsPHENIX Technical Note by the LANL group.

Contents

Chapter 1

Executive Summary

1.1 Executive Summary

In this document we summarize a conceptual design for a forward sPHENIX upgrade, called fsPHENIX, that can address many of the most compelling problems in transverse spin and cold nuclear matter physics. fsPHENIX is designed to carry out a unique program of key measurements that can only be done at RHIC, such as determining the underlying physics mechanism that produces the large transverse single spin asymmetries seen in polarized proton collisions, mapping out gluon saturation at small Bjorken-x in nuclei and studying modifications to the hadronization process, including energy loss, that occur in cold nuclear matter. The resulting data would also provide critical cross checks for future DIS measurements at both JLab and eRHIC, as well as for polarized spin physics theory.

During the last decade, a revolution has occurred in spin physics. From the continuing mystery of the origin of the missing nucleon spin, now known to not be contributed by the gluons alone, to the surprisingly large transverse single spin asymmetries (TSSA) seen at both fixed target and collider experiments, it is clear that there are wide gaps in our knowledge of nucleon and parton spin, including effects from orbital angular momentum.

Two powerful theoretical concepts, now widely accepted by the spin community, namely the Sivers and Collins mechanisms, have been developed to address the origin of single spin asymmetries.

The Sivers function is related to the correlation between the struck parton initial kT direction and the nucleon spin orientation. This function can be measured by determining the angle of the jet axis with respect to the nucleon spin (e.g. the left versus right asymmetry). Once thought to be identically zero, polarized semi-inclusive deep inelastic scattering (SIDIS) measurements by COMPASS and HERMES have shown significant none-zero asymmetries ($A_{UT} \sim 0.05$). The Sivers function is sensitive to the orbital angular momentum (OAM) of the struck parton and vanishes if the OAM is zero. pQCD theory is currently being developed to directly connect the measured Sivers asymmetry to the OAM of the quarks.

The Collins function is related to the correlation between the outgoing jet fragmentation particle's azimuthal angle and the spin orientation of the outgoing quark. Measuring the Collins asymmetry is somewhat more difficult, as it requires precision measurements of the outgoing track relative to the fully reconstructed jet. Non-zero asymmetries for the Collins function have also been observed by both COMPASS and HERMES.

Unfortunately, only a few very limited direct measurements of the Sivers or Collins

asymmetries have been carried out in p+p collisions, due to constraints imposed by the physical detector designs. The existing p+p inclusive single hadron TSSA data likely contain a mixture of both Collins and Sivers effects and cover much larger Bjorken-x values that have minimal overlap with existing data from SIDIS. The theoretical situation for the interpretation of TSSAs is currently in a state of flux. QCD motivated transverse momentum distributions (TMD) (for low pT) and Twist-3 approaches (for large pT) have been developed to study both polarized SIDIS and TSSA pp data, respectively. While doing a fair job of reproducing the magnitude of the data as a function of kinematics, recent theoretical investigation shows that the two frameworks predict opposite signs for the asymmetries! However, only the Sivers function was considered in the treatment of the p+p data, ignoring other possible sources of TSSAs, such as Collins effect.

We propose to study the azimuthal asymmetry of the inclusive jet and charged hadrons inside a jet in transversely polarized p+p (and p+A) collisions at $\sqrt{s} = 200$ GeV, using the fsPHENIX detector at RHIC, thereby providing the first precise determination of the Sivers and Collins asymmetries in those collisions over a wide kinematic region that covers the current SIDIS data of interest. We have optimized the design of fsPHENIX for the measurement of inclusive jets and charged hadrons at forward angles, with high resolution tracking for charged particles and hadronic calorimetry for jets. By covering forward rapidity, this design naturally probes the Bjorken-x range of $x = 0.1 \sim 0.8$ for jet energies between 10 and 80 GeV. This covers the interesting x range that has previously been studied by SIDIS (0.1 to 0.3), allowing the first direct comparison of both the sign and the magnitude of the two types of asymmetries produced in SIDIS with those for p+p. With a p+p integrated luminosity of 50 pb-1, excellent statistical uncertainties can be obtained at several x values for both the Sivers and Collins asymmetries (better than $\sim 0.1\%$). By identifying the charge of the leading hadron in the jet, the scattered quark from the polarized proton can be tagged as an up or down quark with good probability (~ 70 %), which has been successfully demonstrated at other HEP experiments. This method allows for independent measurements of quark flavor identified Sivers asymmetries, which are expected to be larger than those integrate over flavor, as recently measured by the AnDY experiment at RHIC, since the sign of the asymmetries are expected to be opposite for up versus down quarks.

Results from cold nuclear matter studies continue to surprise the heavy-ion physics community. Very large jet energy losses have been observed in peripheral heavy-ion collisions at the LHC, ruling out some models of partonic energy loss in CNM. In addition, a class of rare p+A events have been discovered at the LHC that have very similar flows and multiplicities to those from central heavy ion collisions at RHIC! Two processes have been proposed that could be partly responsible. First is the idea that partonic energy loss approaches a constant fraction of the total incident energy, rather than a fixed (limiting) energy loss value, at very large energies. Second is the possibility that the fragmentation function for a jet traversing CNM is modified. Data for moderate energy jets in p+A collisions from fsPHENIX would play an important role in resolving this puzzle.

fsPHENIX is designed to integrate fully with sPHENIX, by adding a new spectrometer with pseudorapidity coverage from eta of approximately one to four. The detector elements would be identical to, or prototypes for the ePHENIX forward hadron arm, thereby minimizing the cost and ensuring a smooth transition to the eRHIC era. We estimate that this "Stage 1" version of fsPHENIX can be constructed for approximately ten million dollars, perhaps less if ePHENIX prototype or construction funds are available at that time. Thus, this project falls in the category of a DOE Major Item of Equipment (MIE). The

physics reach of fsPHENIX can be be further broadened by the addition of limited electromagnetic calorimetry and a cerenkov detector if funding and time are available. There are other groups (Stony Brook Univ., RIKEN, et al.) currently working on RICH-based hadron particle identification for fs/ePHENIX. The RIKEN group is also interested in building the hadronic calorimeter. The timeline for construction and installation of a Stage 1 fsPHENIX upgrade would provide for data taking during the proposed 2021- 2022 sPHENIX run.

The conceptual design for fsPHENIX is shown in Figure 1. A magnetic field for particle tracking and charge identification is provided by shaping the sPHENIX superconducting solenoid field with a steel piston located around the beam line and an iron return yoke designed as part of the hadronic calorimeter. High resolution tracking near the interaction point is obtained from a reconfigured version of the existing FVTX detector. Three new GEM stations provide intermediate tracking and good momentum determination ($\delta p/p \sim 3\%$ at $p = 10$ GeV/c) for charged particles. A hadronic calorimeter measures total jet energy, position and size. The GEM tracker and hadronic calorimeter are identical in design to those proposed for the ePHENIX forward hadron arm. Note that only these two new detector systems are required for the baseline key physics! Together, they provide jet energy and profile, plus the charge and momentum of the leading hadron. This is adequate to determine both the Sivers and Collins asymmetry at about the " 20% " precision level via global fitting in the x-range of interest, as is demonstrated by simulations shown later in this document. Additional upgrades with a RICH detector and muon identification chambers could provide kaon and photon identification, as well as muon detection, but are not otherwise required.

A short list of the key experimental measurements is given below:

1) Inclusive jet measurements at forward rapidity in transversely polarized p+p collisions at $\sqrt{s} = 200$ GeV, to determine the Sivers asymmetry. The $x1$ coverage (for the transversely polarized proton) is from 0.1 to 0.8, covering and expanding on the kinematics of the existing polarized SIDIS data. The tracking and calorimetry cover eta from 1 to 4, providing a full jet acceptance (center of gravity) from eta of 2 to 3.

2) Sivers asymmetries at the same kinematics for enriched u-quark or d-quark jets, by tagging the jet charge according to the leading hadron's charge. Determine the sign of u-quark and d-quark's Sivers asymmetries in p+p and test the process dependence of Sivers functions. Resolve the "SIDIS and pp" sign mismatch puzzle. Provide theory input for the calculation of quark orbital angular momentum.

3) Azimuthial distributions of charged hadrons inside high energy jets to study the Collins asymmetries. Provide theory input for the global fit of quark transversity distributions.

4) Probe gluon saturation scale QS via charged hadron Collins asymmetry and di-hadron measurements in p+A collisions.

5) Study the modification of jet fragmentation, profile and energy loss in p+A collisions.

These measurements and the corresponding performance simulations are discussed in detail in the main body of this document.

While we discussed only the Stage 1 physics program in above, additional detectors planned for ePHENIX, such as the full Cerenkov and EMCAL, could be installed around the same time to enable additional Stage 2 p+p and p+A physics. For example, the Cerenkov detector would allow particle identification for charged pions, kaons and protons, thereby improving the identification of the struck quark that eventually hadronizes into the observed jet. These particle identified Sivers and Collins asymmetries would provide an important cross check for future SIDIS data from eRHIC. An EMCAL with a preshower

detector would provide for neutral pion and photon measurements, improving the jet energy resolution and adding access to direct photons. The Cerenkov and EMCAL detectors could cover either all or part of the full phi acceptance, depending on funding and availability of ePHENIX prototypes. We note that the jet rates are sufficiently large that detectors with limited phi coverage would still provide useful physics.

To summarize, an exciting program of transverse spin physics in p+p and p+A collisions at RHIC can be performed with a modest investment in a fsPHENIX spectrometer sited at forward angles within the sPHENIX detector. fsPHENIX would use GEM tracking and hadronic calorimetry elements identical to those proposed for ePHENIX, in order to minimize the development time and long term cost to the funding agencies. fsPHENIX would take data simultaneously with sPHENIX and also serve as a excellent testbed for ePHENIX detector development.

Chapter 2

Introduction

Editor: Xiaodong Jiang

2.1 Basic Considerations of fsPHENIX

In 2012, a proposal of super-PHENIX central barrel upgrade [1] was submitted to the BNL management as the future plan of PHENIX upgrade. In summer 2013, the BARBAR solenoid magnet was identified and obtained as the sPHENIX magnet, and in September 2013, PHENIX Collaboration submitted to BNL management a MIE of sPHENIX for the future Heavy Ion program, and a Letter-Of-Intent of ePHENIX detector for the future Electron Ion Collider (EIC) era starting physics production in 2025.

In this document, we describe the forward sPHENIX detector package (fsPHENIX) as an intermediate staged-approach towards the final ePHENIX detector. This approach will provide the flexibility of continues p+p, p+A and A+A physics productions prior to the EIC era, taking full advantages of two decades of heavy investments in RHIC.

In the staged-approach of fsPHENIX, we emphasis the following considerations:

- **Major fsPHENIX sub-detectors should be a part of ePHENIX.** As our final goal is to evolve fsPHENIX into the ePHENIX's hadron-forward arm detector, we explicitly require that all major fsPHENIX sub-detectors satisfy the requirements of ePHENIX.
- **A staged-approach to provide flexibilities under different funding scenarios.** Given the reality of U.S. Nuclear Physics funding, a staged approach of fsPHENIX s illustrated. We emphasize the capability of maintaining readiness of physics data-taking at each stage. A clear evolution path of fsPHENIX into ePHENIX is outlined should EIC construction funding becomes available in the future.
- **Producing the best science under different RHIC operation scenarios.** We illustrate the best scientific cases for fsPHENIX corresponding to different RHIC machine operation and upgrade scenarios to provide realistic options in the years leading towards EIC. **Especially, we highlight the Stage-I physics program for $p^{\uparrow}+p^{\uparrow}$ collision at $\sqrt{s}$=200 GeV, of which data taking can be concurrent with the p+p, p+A and A+A runs of sPHENIX's Heavy Ion Physics program.**

Assumed RHIC machine operation conditions: in illustrating the best scientific cases for fsPHENIX, we have assumed the proton beam's polarization of $P_b = 0.60$, and the ex-

perimental recorded luminosities corresponding to the following different RHIC operation scenarios, within a vertex cut of ±30 cm:

Stage-I, concurrent with sPHENIX running:

- $\mathcal{L} = 50$ pb^{-1} in $p^{\uparrow} + p^{\uparrow}$ collisions at $\sqrt{s}$=200 GeV.
- $\mathcal{L}_{NN} = 50$ pb^{-1} in $p^{\uparrow}$+Au collisions at $\sqrt{s}$=200 GeV.
  (Equivalent nucleon-nucleon luminosity.)

Stage-II of fsPHENIX in the future will include:

- more $p + p$ and $p + A$ collisions at $\sqrt{s}$=200 GeV.
- $p^{\uparrow} + p^{\uparrow}$ and $\vec{p} + \vec{p}$ collisions at $\sqrt{s}$=510 GeV.

2.2 Science Highlights of fsPHENIX

Understanding the Origin of Nucleon Spin: The fsPHENIX's physics program will help us obtain detailed knowledge to answer the following questions:

- **A detailed knowledge of valence quarks' transverse momentum dependent parton distributions (TMDs) such as the Sivers and the transversity distributions**. The naive T-Odd quark Sivers distribution functions arises from the imaginary piece of interference between angular momentum L= 0 and L≠ 0 quark wave-functions, therefore is related to quarks' orbital angular motion.
- **Clearly verify the fundamental QCD prediction of the process dependency of quark Sivers functions.**
- **How much transverse spin (transversity) does each flavors of valence quark carry in a transversely polarized nucleon ?**

Understanding the Properties of Cold Nuclear Matter (CNM):

- **How does the nuclear environment affect the distribution of gluons inside a nuclei?**
- **Where does the saturation of gluon densities set in?**
- **What is the energy loss of quarks in CNM ?**
- **Is the jet fragmentation process modified in CNM ?**

Highlight Plots:
Forward jet left-right asymmetry A_N, and the variation of A_N with enhancement of different quark flavor contributions.
Forward charged hadron.
Hadron azimuthal distribution inside a jet.
Recoil Λ polarization ($\Lambda^{\uparrow} \to \pi^{-} p$)
J/ψ, ψ'.
R_{pA}.

2.3 fsPHENIX, a Two-Staged Approach: Detector Overview

To provide flexibilities in construction schedule and funding while at the same time providing maximum physics outputs, we present a staged-approach in constructing the fsPHENIX detectors.

The layout of the Stage-I fsPHENIX detector design is shown in Fig. 2.1. These detectors are identical to the corresponding parts in the proposed ePHENIX's hadron-forward arm detector.

The fsPHENIX detector designs are aimed at achieving (dummy draft)

- Tracking resolution specifications.
- Jet reconstruction specifications.
- Particle Identification specifications.

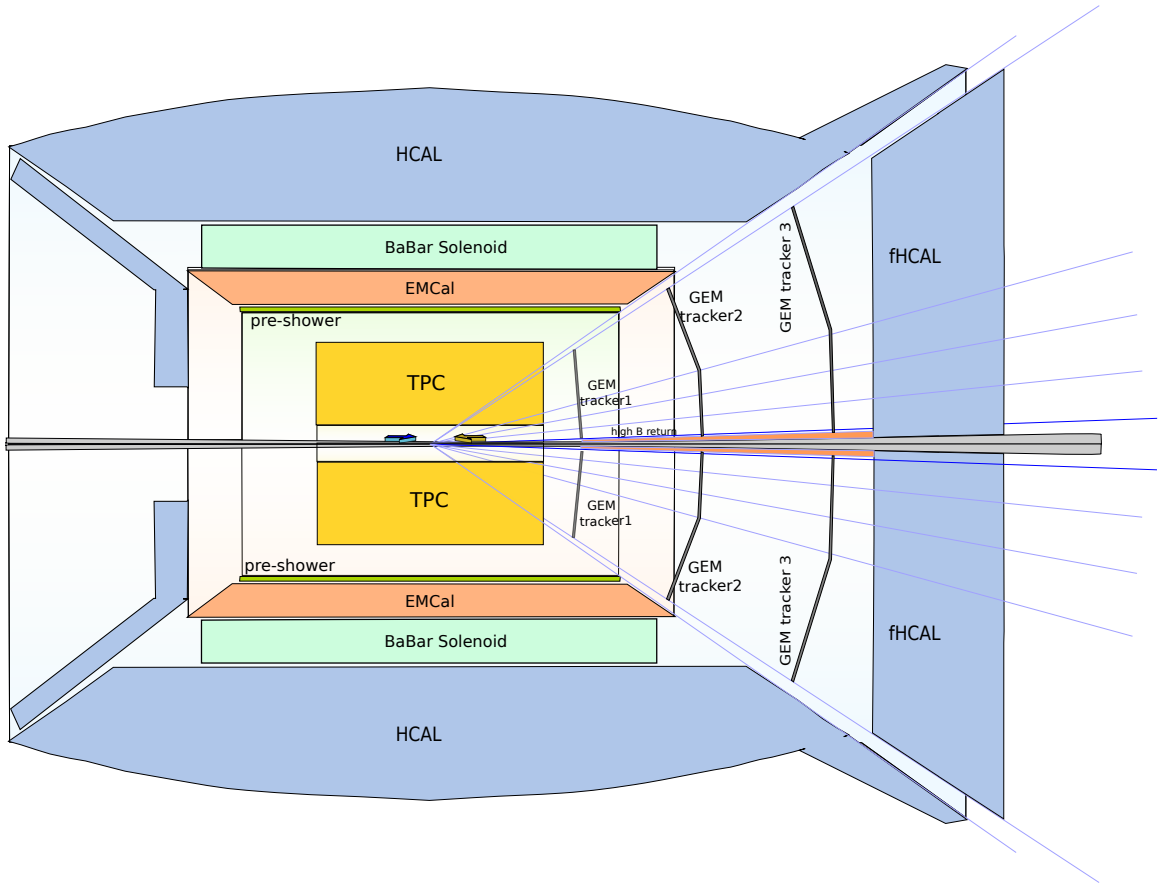

Figure 2.1: The layout of the Stage-I forward sPHENIX design, including three GEM tracking stations (GEM1-GEM3) and a forward Hadronic Calorimeter (fHCal)

2.4 Experimental Observables, Physics Deliverables and Required Detectors for fsPHENIX Stage-I

A summary physics topics, observables, required detectors are listed in Table 2.1 for Stage-I

	Observable	Physics	Detectors Required						Costs
			FVTX	GEMTr	hPID	EMCal	HCal	MuID	
$p^{\uparrow}+p^{\uparrow}$	incl. A_N^{Jet}	Quark Sivers	×	√	×	×	√	×	
200 GeV	$A_N^{h^{\pm}-Jet}$	Collins $\delta q(x)$	×	√	×	×	√	×	
50 pb^{-1}	Interf. A_N^{2h}	Transv. $\delta q(x)$	×	√	×	×	√	×	
	$\Lambda^{\uparrow}$ pol.	Transv. $\delta q(x)$	×	√	×	×	√	×	
$p^{\uparrow}+A$	$A_N^{h^{\pm}-Jet}$	Collins in Nucl.	×	√	×	×	√	×	
200 GeV	A_N^{h+}, A_N^{h-}	Saturation	×	√	×	×	√	×	
50 pb^{-1}	di-jets	$g_A(x,Q^2)$, CNM	×	√	×	×	√	×	
50 pb^{-1}	incl. R_{pA}^{Jet}	CNM	×	√	×	×	√	×	

Table 2.1: Stage-I fsPHENIX selected measurement observables, accessible physics topics, and required detectors (draft).

2.4.1 Unique kinematic advantages of fsPHENIX

A few key plots, x_1 vs x_2 coverage comparison with STAR-2017, for forward jets.
Access of valence quarks x_1, sea quarks and gluons (x_2).
Uniqueness of fsPHENIX kinematic coverage compared with fixed target experiments COMPASS, FNAL Drell-Yan E-1027, E-1039. Compared with coverage of existing PHENIX and STAR.

	Observable	Physics	Detectors Required						Costs
			FVTX	GEMTr	hPID	EMCal	HCal	MuID	
$p^\uparrow + p^\uparrow$	incl. A_N^{Jet}	Quark Sivers	×	×	×	×	√	×	
200 GeV	$A_N^{h^\pm - Jet}$	Collins $\delta q(x)$	×	√	×	×	√	×	
50 pb^{-1}	Interf. A_N^{2h}	Transv. $\delta q(x)$	×	√	×	×	√	×	
	$A_N^{\pi - Jet}$	Collins $\delta q(x)$	×	√	π √	×	√	×	
	$A_N^{K - Jet}$	Collins $\delta s(x)$	×	√	K √	×	√	×	
	$\Lambda^\uparrow$ pol.	Transv. $\delta q(x)$	×	√	×	×	√	×	
	prom. A_N^γ	Quark Sivers	×	×	×	√	√	×	
$\vec{p} + \vec{p}$	incl. A_{LL}^{Jet}	$\Delta q(x_1)\Delta g(x_2)$	×	×	×	×	√	×	
200 GeV	prom. A_{LL}^γ	$\Delta q(x_1)\Delta g(x_2)$	×	×	×	√	√	×	
50 pb^{-1}	$A_{LL}^{\gamma - Jet}$	$\Delta q(x_1)\Delta g(x_2)$	×	×	×	√	√	×	
	A_{LL}^{h+}, A_{LL}^{h-}	$\Delta g(x)$ sign	×	√	×	×	√	×	
$p^\uparrow + A$	$A_N^{h^\pm - Jet}$	Collins in Nucl.	×	√	×	×	√	×	
200 GeV	$A_N^{\pi+}$, $A_N^{\pi-}$	Saturation	×	√	π √	×	√	×	
50 pb^{-1}	incl. R_{pA}^{Jet}	CNM	×	×	×	×	√	×	
	prom. R_{pA}^γ	Gluon $g_A(x)$	×	×	×	√	√	×	
	DY $R_{pA}^{\mu\mu}$	CNM	√	√	×	×	√	√	
$p^\uparrow + p^\uparrow$	DY $A_N^{\mu\mu}$	Quark Sivers	√	√	×	×	√	√	
510 GeV	DY A_N^{ee}	Quark Sivers	√	√	×	√	√	×	
300 pb^{-1}	DY $A_{TT}^{\mu\mu}$	$\delta q(x_1)\delta\bar{q}(x_2)$	√	√	×	×	√	√	
	DY A_{TT}^{ee}	$\delta q(x_1)\delta\bar{q}(x_2)$	√	√	×	√	√	×	
	prom. A_N^γ	Quark Sivers	×	×	×	√	√	×	
$\vec{p} + \vec{p}$	DY $A_{LL}^{\mu\mu}$	$\Delta q(x_1)\Delta\bar{q}(x_2)$	√	√	×	×	√	√	
510 GeV	DY A_{LL}^{ee}	$\Delta q(x_1)\Delta\bar{q}(x_2)$	√	√	×	√	√	×	
300 pb^{-1}	incl. A_{LL}^{Jet}	$\Delta q(x_1)\Delta g(x_2)$	×	×	×	×	√	×	
	prom. A_{LL}^γ	$\Delta q(x_1)\Delta g(x_2)$	×	×	×	√	√	×	
	$A_{LL}^{\gamma Jet}$	$\Delta q(x_1)\Delta g(x_2)$	×	×	×	√	√	×	

Table 2.2: (xxx.xx Saved here, for future editions, xj) . Stage-II fsPHENIX selected measurement observables, accessible physics topics, and required detectors in each measurement corresponding to recorded luminosities of 50 pb^{-1} for p+p at 200 GeV, 50 pb^{-1} nucleon-nucleon equivalent luminosity for p+A at 200 GeV, and 300 pb^{-1} for p+p 510 GeV within the vertex range of ± 30 cm.

Chapter 3

Studies of Nucleon Spin Structure Through Polarized p+p Collisions

Editor: Xiaodong Jiang

3.1 Introduction: puzzles in spin physics and the goal of fsPHENIX.

The Puzzle of "Missing-Spin" : Several decades of experiments on deep inelastic scattering (DIS) have provided us with detailed information on how partons (quarks and gluons) share the momentum of a fast-moving nucleon. However, we do not have a clear answer to the question of how partons share the nucleon's 1/2- spin. The puzzle of nucleon's "missing-spin" has been hunting theorists and experimentalists alike since the mid-1980's [2]. In the framework of Jaffe-Manohar [3], the decomposition of nucleon's 1/2-spin [4] has a partonic interpretation as:

$$\frac{1}{2} = \frac{1}{2}\Delta\Sigma + \Delta G + L_q + L_g, \tag{3.1}$$

with contributions from quark and gluon's spin ($\Delta\Sigma$ and ΔG), and their orbital angular momentum (L_q and L_g) [5].

From global fits of polarized DIS data [6], the current knowledge put the quark-spin ($\frac{1}{2}\Delta\Sigma$) term at only 25-35% of the proton's spin, much less compared to the naive parton model expectation. While there has been experimental indications of non-vanishing gluon polarization, the current knowledge based on double-spin asymmetry of jet and neutral pion data from RHIC [7] puts ΔG term's contributions at $\int_{0.05}^{0.2} \Delta g(x)dx = 0.005 \pm^{0.129}_{0.164}$ at a scale of $Q^2 = 10$ GeV^2, leaving a significant portion of proton's spin not accounted for, presumably from parton's orbital angular momentum (OAM).

The Puzzle of Large Single-Spin Asymmetries in $p+p$ Collision : In addition to the "missing spin" puzzle, there's been another long-standing unexplained spin phenomenon, namely, the observed large single-spin asymmetries (SSA), at 20-40% level, in $p^{\uparrow}+p \to \pi+X$ reaction over a broad range of $\sqrt{s}$. Collinear perturbative QCD at leading-twist [8], which predicted SSA's are of the order of $\alpha_s(m_q/\sqrt{s})$ (where m_q is the quark mass) and thus very small, simply could not explain such a large SSA. Furthermore, xxx.xx Λ polarization xxx.xx. Two-types of theoretical frameworks have been developed over the past two decades

in efforts to resolve the large SSA puzzle: the transverse momentum dependent (TMD) factorization framework and the collinear twist-3 factorization framework.

Within the TMD factorization framework, at low transverse momenta $P_{hT} \ll Q$, naive time-reversal odd TMD parton distribution (Sivers distribution) or fragmentation function (Collins fragmentation function) were introduced in order to explain the large SSA. The Sivers effect (or Sivers parton distribution) correlates quark's transverse momentum with nucleon's transverse spin to generate a left-right bias. The Collins effect, on the other hand acting as a "quark polarimeter", couples the quark's transverse spin (transversity h_1) with spin-dependent fragmentation functions ($H_1^\perp$) to generate a left-right bias. In inclusive single hadron SSA in pp, which involves only one hard scale hadron p_t, contributions from both Sivers effect and Collins effect are mixed. However, these two TMD related effects can be separated in processes that explicitly involve two scales, such as in semi-inclusive deep-inelastic scattering (SIDIS), or polarized proton collisions that produce jets, final state polarization, correlated di-hadron pairs, or Drell-Yan lepton pairs.

Within the collinear twist-3 factorization framework, at high transverse momenta $P_{hT} \gg M$, SSAs arise from twist-3 quark gluon correlator the so-called Efremov-Teryaev-Qiu-Sterman function (ETQS) [9, 10, 11, 12], tri-gluon correlation functions [13, 14], or twist-3 collinear fragmentation functions [15]. The two approaches, TMD factorization schemes and collinear twist-3 factorization scheme, are also shown to be related to each other [16, 15]. In the intermediate transverse momentum region ($\Lambda_{QCD} \ll p_T \ll Q$) where both approaches apply, they were shown to be consistent.

The Collins and the Sivers effects can be clearly separated through azimuthal angular dependence of SSA measured in semi-inclusive deep-inelastic scattering (SIDIS) reactions with a lepton beam. It has been an extensive world-wide effort over the last decade to measure SSA in SIDIS reactions. The HERMES experiment at DESY carried out the first SSA measurement in SIDIS reaction on a transversely polarized proton target [17, 18]. The COMAPSS experiment at CERN carried out similar SSA measurements on transversely polarized deuteron and proton targets [19, 20], and Jefferson Lab Hall A published results of SSA measurements on a transversely polarized neutron (^{3}He) target [21]. These experiments confirmed that both Collins and Sivers effects are significant, such that quark transversity and Sivers distributions are clearly non-vanishing. Furthermore, quark transversity and Sivers distributions are demonstrated to have very strong flavor dependencies, u-quark and d-quark have opposite signs in both cases.

The quark Sivers distribution [22], which represents a correlation between quark's transverse momentum and nucleon's spin, arises from the final state gluon exchange between the struck quark and the nucleon remnant in SIDIS, or from initial state interactions in Drell-Yan process, is shown to be non-vanishing [23]. Taking gauge links into consideration, Sivers distribution is predicted to be process dependent in the sense that it differer by a sign from SIDIS to Drell-Yan process [24, 23]. Furthermore, Sivers distribution requires the nucleon helicity to be flipped from the initial state to the final state, thus involves two different quark angular momentum components in the wave function. The same matrix element appears in Sivers distribution as in the nucleon's Pauli form factor quark-by-quark, thus one can correlate the Sivers asymmetry for each quark with the anomalous magnetic moment of the nucleon carried by that quark [25], therefore explains the opposite behavior of valence up-quark and down quarks observed in pp and SIDIS.

The quark transversity distribution, denoted by $h_{1q}(x, Q^2)$, which are equally fundamental at leading twist as the parton density $f_{1q}(x, Q^2)$ and helicity distribution $g_{1q}(x, Q^2)$. The chiral-odd transversity quark distribution $h_{1q}(x, Q^2)$ measure the difference of the probabil-

ities to find a quark with its spin parallel to that of a transversely polarized nucleon and of finding it oppositely polarized. Unlike the case of unpolarized and longitudinally polarized densities, there is no gluon transversity distribution at leading twist due to angular momentum conservation and the $h_{1q}(x, Q^2)$ are not accessible in inclusive DIS measurements because of their chirality properties. Experimental observation of quark transversity effects need to chose observables in which $h_{1q}(x, Q^2)$ is coupled with another chiral odd object, either a chiral-odd parton distribution or chiral odd fragmentation functions. For example, couple with another transversity distribution or Bore-Moders parton distribution for example in polarized Drell-Yan reactions, or couple to a chiral odd fragmentation function such as the spin-dependent quark to hadron Collins fragmentation function, two-hadron interference fragmentation functions, or spin transfer fragmentation functions (i.e. final state Λ transverse polarization) in semi-inclusive DIS or in pp collisions.

Thus, to clearly understand quark transversity and Sivers distribution has become one of the main goals in the field of spin physics, and a consistent QCD-based picture of SSA effects in SIDIS and hadronic production has become a key issue. In the coming years, with JLab-12 GeV upgrade currently underway, and several SIDIS spin experiments already planned to obtain SSA data on proton and neutron (3He) targets (cite Hall A, Hall B experiments) covering the valence quark region of $0.12 < x < 0.5$, with $1.0 < Q^2 < 4.0$ GeV^2, it is crucial to obtain SSA data from hadronic collisions covering a similar x-region (even to a higher x-region), but at a much higher hard-scattering energy scale ($10 < Q^2 < 50$ GeV^2).
The Major Challenges : the major challenges currently facing spin physics, specifically spin-physics in hadronic-collisions are:

- **A significant amount of nucleon's 1/2-spin can not be accounted for.** Although there're indications that parton's orbital angular momentum should make up the missing spin of proton, we do not know their detailed structures vs flavor and momentum fraction (x).

- **Large transverse single-spin asymmetries observed in hadronic collisions can not be well-explained.** Due to the fact that two competing effects, initial state (Sivers) vs final state (Collins) effects, can not be distinguished in inclusive hadron SSA measurements.

- **There's no well-established consistent explanation to reconcile SSA effects observed in SIDIS and hadronic collisions.** For example, even the sign of valence quark Siverve distributions extracted from SIDIS and from hadronic collisions disagrees.

- **Our current knowledge on quarks' transverse spin (transversity) and Sivers distributions (TMD) only comes from SIDIS experiments.** There's been no independent confirmations from hadronic collisions to independently verify the universality of these parton distributions in different processes. Key QCD predictions, such as Sivers function process dependence between SIDIS and inclusive jet, inclusive prompt photon and Drell-Yan processes in hadron collisions has not been verified.

3.1.1 The Goals of fsPHENIX in Spin Physics at Stage-I

With a hadronic calorimeter (HCal) to provide jet energy and jet center determinations, plus the reconfigured FVTX and three GEM tracking stations to measure the charge-sign

and momentum of charged hadrons, at the Stage-I of fsPHENIX, we emphasis on the capability of identifying forward jet events and tag the charge sign of leading hadrons in $p^{\uparrow} + p \to jet + X$ reaction at $\sqrt{s} = 200$ GeV, and extracting charged hadron azimuthal distributions inside a reconstructed jet. The main physics goals include:

- **Inclusive jet single-spin (left-right) asymmetry** A_N^{jet}. Which is purely sensitive to quark Sivers distributions from the combined effects of u-quark and d-quark.
- **Leading hadron charge sign tagged jet single-spin asymmetry** A_N^{T-jet}. Which is purely sensitive to quark Sivers distributions, but with different combination effects from u-quark and d-quark. Relatively speaking, positively charge-tagged jets contain more contributions from u-quark, while negatively charge-tagged jets add more contributions from d-quark.
- **Charged hadron azimuthal distributions inside a jet** A_N^{h-jet}**.** Which is purely sensitive to quark transversity distributions coupled to the chiral-odd quark-to-hadron Collins fragmentation functions. In a consistent picture with SIDIS data, one expects that positively and negatively charged hadrons have opposite signs and z-dependencies in A_N^{h-jet} from the current understanding that the favored and the un-favored Collins fragmentation functions are opposite in sign.
- **Di-hadron correlated azimuthal asymmetry** A_N^{2h}**.** Which is purely sensitive to quark transversity distributions coupled to the chiral-odd di-hadron interference fragmentation functions (IFF). Due to the detailed properties of IFF, one expects different amplitudes, z-dependencies and signs of A_N^{2h} for different charged hadron combinations.
- **Transverse** Λ **(and** $\bar{\Lambda}$**) final state polarization in** $p^{\uparrow} + p \to \Lambda^{\uparrow}(\bar{\Lambda}^{\uparrow}) + X$. Which is purely sensitive to quark (or anti-quark) transversity coupled with spin-transfer fragmentation functions which can be accessed through $e + e-$ data.

Other spin observables in fsPHENIX Stage-I: When combined with sPHENIX central barrel's capabilities of jet and prompt photon reconstruction, single-spin and double-spin observable of types like: 2-jets, γ-jet, and hadron-jet become accessible in transverse as well as longitudinal polarized p-p collisions at 200 GeV. This type of unique capabilities will open up new opportunities, for example, to provide additional handles on quark and gluon polarizations in different kinematic range.

In the following sections, we give detailed descriptions of each physics cases, in transverse spin and in longitudinal spin physics, underlining the uniqueness of fsPHENIX's capabilities. **We highlight the Stage-I physics program of $p^{\uparrow} + p^{\uparrow}$ collision at $\sqrt{s}$=200 GeV, of which data taking can be concurrent with the pp reference run of sPHENIX's Heavy Ion Physics program.**

3.2 Current Challenges in Transverse Spin Physics

Since the observation of surprisingly large single transverse spin asymmetries (SSAs) in $p^{\uparrow} + p \to \pi + X$ reactions first at ZGS in 1970s [26], then in 80s-90s at BNL [27] and Fermilab [28], the exploration of the physics behind the observed SSAs has become a very active research branch in hadron physics, and has played an important role in our efforts to

understand QCD and nucleon structure. The large SSA observed over a wide range of $\sqrt{s}$ has been summarized [29] in Fig. 3.1. The field of transverse spin physics has now become the most active area in high energy nuclear physics, generating tremendous excitement on both theoretical and experimental fronts. Over the last decade, new single-spin asymmetry data has become available in inclusive hadron, inclusive jet and di-hadron correlation from high energy pp collisions at RHIC, and from SIDIS experiments at CERN, DESY and JLab. In this section, we briefly discuss the existing single-spin asymmetry data in pp and in SIDIS and their interpretations, and outline the current challenges in transverse spin physics.

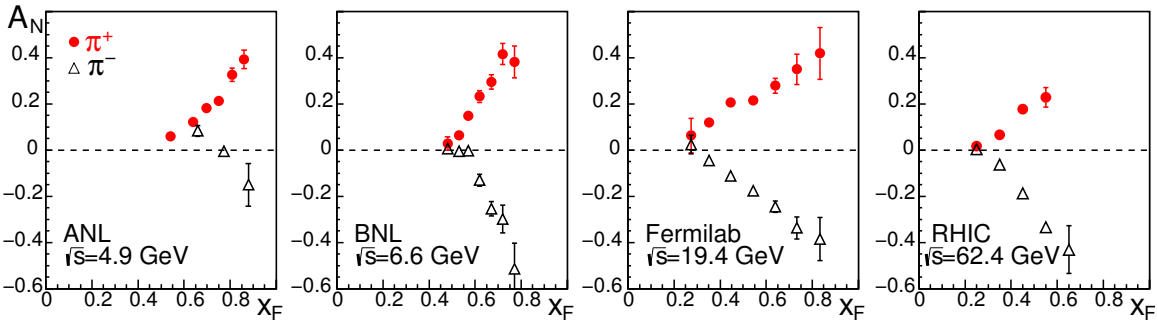

Figure 3.1: The transverse single spin asymmetry in forward $\pi^{\pm}$ production as measured in polarized proton-proton collisions across a range of center-of-mass energies [29] . From left to right, the data are from [26], [27], [28], and [30]. Error bars are statistical errors only.

3.2.1 Inclusive Hadron Single-Spin Asymmetries

Fermilab E704's observation of large SSA [28] initially presented a challenge for QCD theorists and contradicted the general expectation from pQCD of vanishingly small SSA assuming it is originated from a helicity flip of a collinear parton. It was even more startling that the SSA discovered by E704 at $\sqrt{s} = 19.4$ GeV did not vanish at all, as expected from pQCD, at the much higher $\sqrt{s}$ of 62.4 GeV and 200 GeV from the BRAHMS [30] for charged pion and the PHENIX and STAR [31, 7] experiments for neutral pion production, as shown in Figure 3.2. Although theory calculations based on a fit [32] of Sivers Transverse Momentum Dependent parton distributions (TMD) and a twist-3 calculation [33] roughly described the x_F dependencies of SSAs, they failed to describe the trend of transverse momentum (p_T) dependencies of SSA. PHENIX preliminary results [34] of forward "single-cluster" MPC hits (presumably π^0s) SSA A_N at $\sqrt{s} = 200$ GeV also showed similar large size asymmetries. In addition, sizable SSA have also been observed in various inclusive hadron production channels [35] at $\sqrt{s} = 200$ GeV, such as in η^0, K^+, K^-, proton or anti-proton production [30]. Even at $\sqrt{s} = 510$ GeV, STAR preliminary results [36] confirmed that π^0 SSA remains at a few % level. It was also observed by E704 that $\Lambda(uds)$ hyperon production [37] carries a significantly negative single-spin asymmetry within $0.3 < x_F < 0.8$ at $\sqrt{s} = 19.4$ GeV. The existence of these large single spin asymmetries at very forward rapidities at RHIC gives hope that transverse spin phenomena in polarized pp collisions at RHIC can be used as a tool to probe the correlation between parton's transverse motion and the nucleon's spin in order to provide a 3-dimensional dynamical image of the nucleon.

xxx.xx More Comments on factorization here: xxx.xx However, it should additionally be noted that for processes involving hadron production in hadronic collisions, it has been

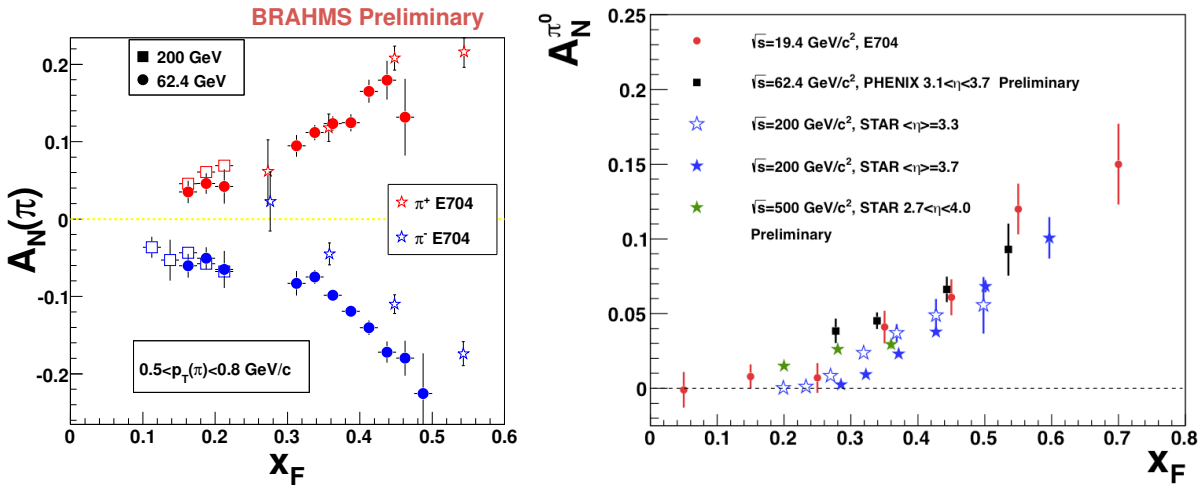

Figure 3.2: Left panel: single spin asymmetry A_N of charged pion production at $\sqrt{s} = 62.4$ and 200 GeV from BRAHMS [30] compared with E704 SSA data [28] at $\sqrt{s} = 19.4$ GeV. Right panel: π^0 meson SSA as a function of Feynman x_F, measured at the STAR and PHENIX experiment in $p + p$ collisions at $\sqrt{s} = 62.4, 200, 500$ GeV [7].

predicted that when the transverse momentum of the partons is taken into account, long-distance structure cannot be factorized into distributions describing partons in separate hadrons, and the partons become entangled across hadrons [38]. This breakdown of factorization for transverse-momentum-dependent functions recently led to the prediction of additional spin asymmetries in hadron-hadron collisions [39]. Further theoretical and phenomenological development will be needed before any calculations based on these ideas can be compared to asymmetries for hadron production in proton-proton collisions.

3.2.2 Hadron Azimuthal Distribution Asymmetries within a Jet

Although Collins and the Sivers effects can not be separated in inclusive hadron SSA in $p + p$ collisions in which only one hard scale (jet $p_\perp$) is involved, however, in processes involved two-hard scales, for example in hadron azimuthal distribution within a jet, $\phi_h - \phi_S$ as illustrated in the left panel of Fig. 3.3, Collins effect can be clearly isolated in which a Chiral-Odd spin-dependent Collins fragmentation function is coupled to the quark transversity distribution [40]. The preliminary STAR result [41, 42] of this observable for identified charged pions in central rapidity (with jet $p_\perp > 10$ GeV) as a function of z_π ($z_\pi = p_\pi / p_{jet}$) is shown in the right panel of Fig. 3.3. Although with limited statistical precision, a trend of opposite sign asymmetry for positive and negative charged pions can be seen, this observation is consistent with that from SIDIS Collins SSA data of HERMES and COMPASS.

3.2.3 Di-Hadron Correlation Single-Spin Asymmetry within a Jet

Quark transversity distributions can also be accessed through the di-hadron correlated single-spin asymmetries within a jet in $p^\uparrow + p$ collisions [43, 44] in which the Chiral-Odd di-hadron spin-dependent interference fragmentation function (IFF) is coupled to the Chiral-Odd quark transversity distributions. In the di-hadron correlated observable, the vector of

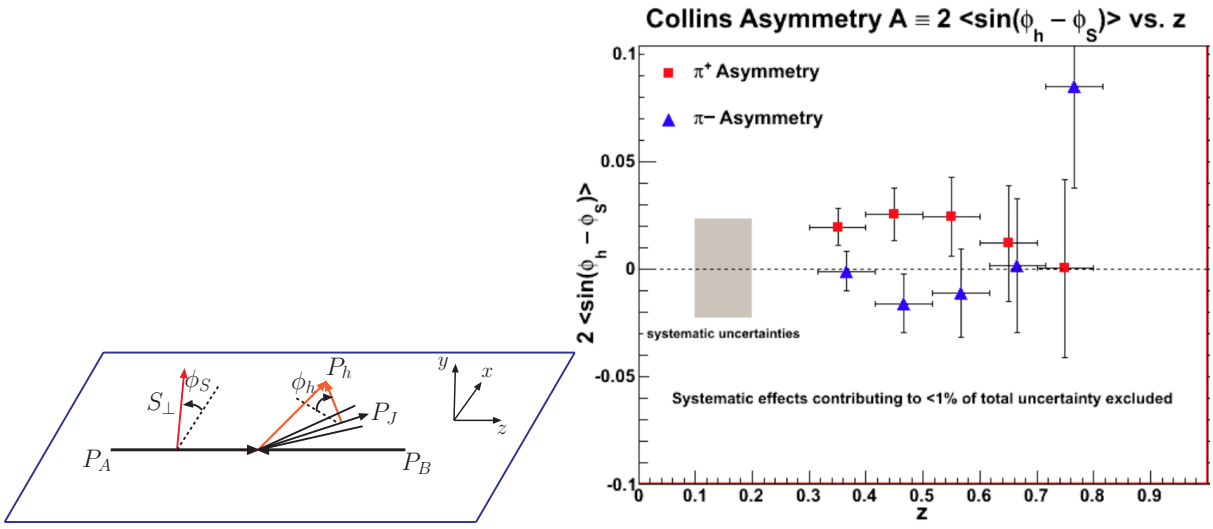

Figure 3.3: Left panel: an illustration of azimuthal angle ϕ_h and ϕ_S. Right panel: STAR preliminary results of charged pion azimuthal distribution asymmetries inside a jet [41].

the momentum difference between the observed two-hadron $\vec{R} = \vec{P_{h1}} - \vec{P_{h2}}$ replace the role of P_h in left panel of Fig. 3.3. The IFF can be accessed through e^+e^- data, and it was shown by the BELLE Collaboration that that the spin-dependent IFF of charge-ordered $\pi^+\pi^-$ pairs is significantly non-zero [45].

PHENIX Collaboration presented preliminary mid-rapidity di-hadron correlated SSA based on 2006 and 2008 transverse run data [46], as shown in Fig. 3.4. It is expected that at forward rapidity, where the valence quarks transversity distributions play more dominate roles, the di-hadron correlated SSA should be sizable. Similar di-hadron correlated SSA has been reported in SIDIS measurements for $\pi^+\pi^-$ pairs by the HERMES [47] and for h^+h^- pairs by the COMPASS [48] Collaborations, and a theory model [49] of IFF with a phenomenology fit [50] of SIDIS data also indicated that di-hadron IFF can be non-zero, thus it is hopeful that IFF can be used to extract quark transversity distributions in pp collisions.

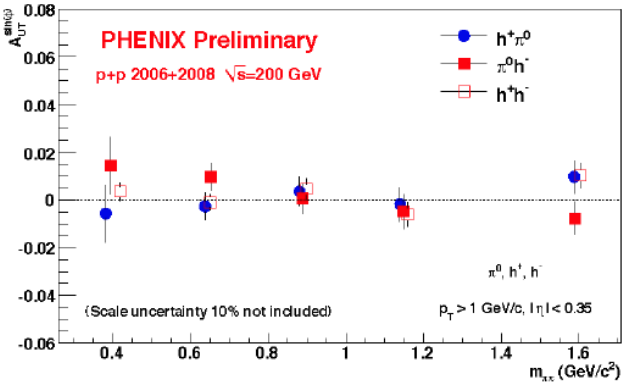

Figure 3.4: Single spin asymmetries of correlated hadron pairs measured by the PHENIX experiment in pp collision at $\sqrt{s} = 200GeV$ at RHIC [46], as a function of invariant mass of the di-hadron pair.

3.2.4 Inclusive Jet Single-Spin Asymmetries in $p^{\uparrow} + p$

Sivers effect in $p + p$ collision can be clearly isolated in inclusive jet left-right single-spin asymmetry A_N^{jet}, since the quark transverse spin effect (Collins effect) is averaged out when integrating over hadron azimuthal angles with respect to the jet axis. A_NDY experiment at RHIC [51] recently reported inclusive jet SSA at $\sqrt{s} = 500$ GeV at the forward rapidity $\langle \eta_{jet} \rangle = 3.25$, as shown in Fig. 3.5. The measured small and positive jet A_N is naively expected since inclusive hadron SSA roughly follow $A_N^{\pi^+} \approx ? A_N^{\pi^-}$, thus giving canceling contributions from $\pi^{\pm}$ in a jet.

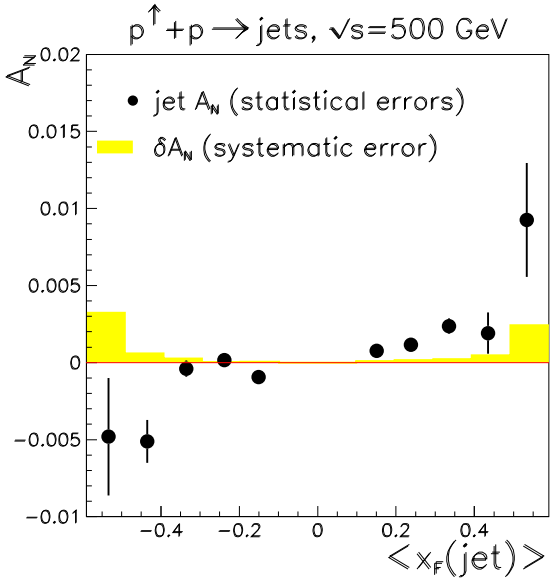

Figure 3.5: A_NDY experiment's inclusive jet single spin asymmetries in $p + p$ collision at $\sqrt{s} =$ 500 GeV and $\langle \eta_{jet} \rangle = 3.25$ at RHIC [51], as a function of x_F. Systematic error estimates do not include scale uncertainty from the beam polarization measurements.

A_NDY's particle detection was relied on calorimeter alone (HCal, partial data with additional ECal) which could not provide detailed information on each particle's momentum vector and charge. Therefore, A_NDY's jet-finding algorithm were based on calorimeter hit pattern and energy deposit. Varying the jet finder algorithm and valid jet parameters led to the dominate systematic uncertainties, at the level of 3×10^{-3}, as shown by the yellow bands in Fig. 3.5. In comparison, false asymmetries of A_N^{jet}, for example introduced from relative luminosity corrections, were shown to be less than 2×10^{-4}.

Interpretations of jet A_N.

Process dependency of Sivers function. Jet A_N interpretations Gamberg et al. [52].

Predictions of Anselmino *et al.* [53], is shown in Fig. 3.7, with combined up- and down-quark effect (left) and separated up- and down quark contributions (right).

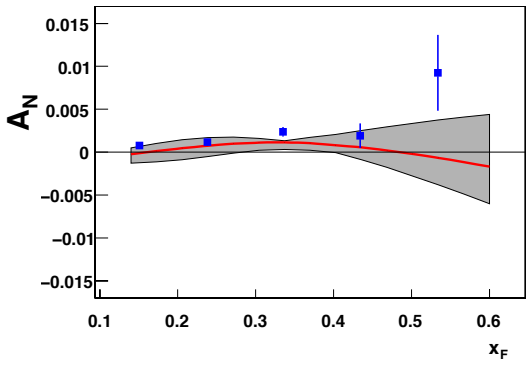

Figure 3.6: Predictions [52] of jet A_N using Sivers function from SIDIS data compared with data of the AnDY experiment [51].

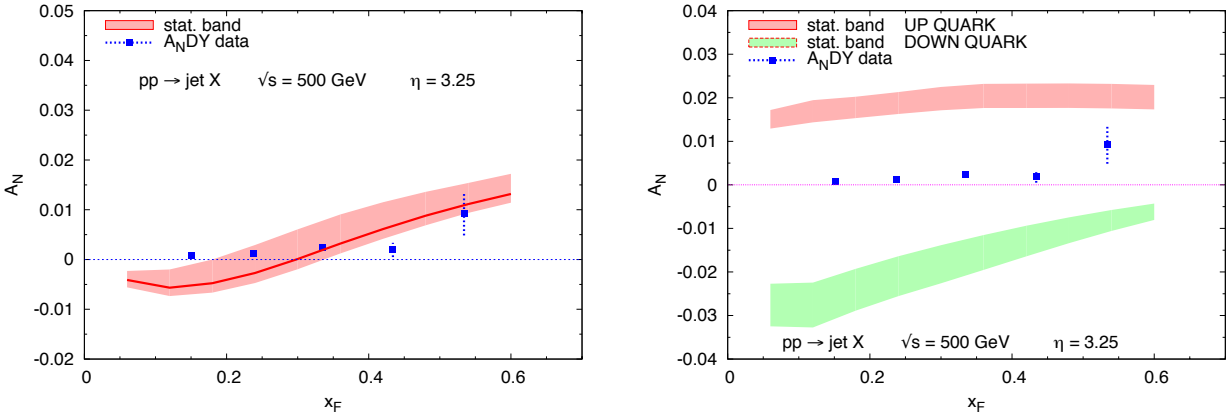

Figure 3.7: Predictions [53] of jet A_N using Sivers function from SIDIS data compared with data of the AnDY experiment [51]. Left panel: combined up- and down-quark effects. Right panel: separated contribution from up-quark (red band) and down-quark (green band).

3.2.5 Hyperon Induced Polarization and Polarization Transfer in pp

Induced Hyperon Polarization

Polarization Transfer

3.2.6 Single-Spin Asymmetries in Deep Inelastic Scattering

The Collins and the Sivers effects, although not possible to be separated in inclusive hadron SSA in $p + p$ collisions, can be clearly separated through azimuthal angle dependence of SSA measured in semi-inclusive deep-inelastic scattering (SIDIS) reactions. It has been a world-wide effort over the last several years to measure SSA in SIDIS reactions. The HERMES experiment at DESY carried out the first SSA measurement in SIDIS reaction on a transversely polarized proton target [17, 18], the COMAPSS experiment at CERN carried out similar SSA measurements on transversely polarized deuteron and proton targets [19, 20, 54], and Jefferson Lab Hall A published results of SSA measurements on a transversely polarized neutron (^{3}He) target [21].

After accounting for the differences in kinematic factors, the Collins SSA of proton from COMPASS and HERMES agree reasonably well in the overlapping kinematic region, and show clear non-zero SSA for both positively and negatively charged hadrons. One finds the striking observation that the Collins amplitude for π^+ is of similar size to π^- production but comes with opposite sign. This hints at an unfavored spin-dependent Collins fragmentation function of similar size and opposite sign to that of the favored one, a situation very different from that observed with unpolarized fragmentation functions.

Clear non-zero Sivers SSA have also been observed by COMPASS in positive hadron production [55]., π^+ in HERMES [56], on proton targets. COMPASS negative hadron SSA, π^- in HERMES, are consistent with zero. COMPASS deuteron [20] π^+ and π^- Sivers SSA, which is consistent with zero, HERMES and COMPASS Sivers asymmetry data indicated that up-quark and down-quark Sivers distributions are opposite in sign. This observation has been further confirmed by the JLab Hall A polarized neutron (^{3}He) target SSA data [21]. Such pronounced flavor dependence of the quark Sivers functions were also indicated by a phenomenological fit [**?**] of the published proton and deuteron Sivers SSA data.

3.2.7 Quark transversity distribution and Collins fragmentation function extracted from global fit of SIDIS data

The observed non-zero Collins asymmetry in SIDIS, which is related to the convolution products of the chiral-odd quark transversity distribution [57] with another chiral-odd object the "Collins Fragmentation Function", strongly indicated that both the quark transversity as well as the quark to hadron Collins fragmentation functions are non-vanishing. The similar amplitudes and the opposite signs of positive-hadron SSA relative to that of the negative hadron indicated that the the up-quark transversity is opposite to that of down-quark, but similar in amplitudes, and the "unfavored" Collins fragmentation function is opposite in sign to that of the "favored" one, perhaps with an even larger amplitude. Independently, the convoluted effect of two non-zero Collins fragmentation functions has been observed by the BELLE Collaboration [58], and recently by the BARBAR Collaboration [59] in $e^+e^- \to h_1h_2X$ process. The quark to hadron Collins fragmentation function together with the quark transversity distributions have been extracted simultaneously from these data [60, 61], as shown in Fig. 3.8.

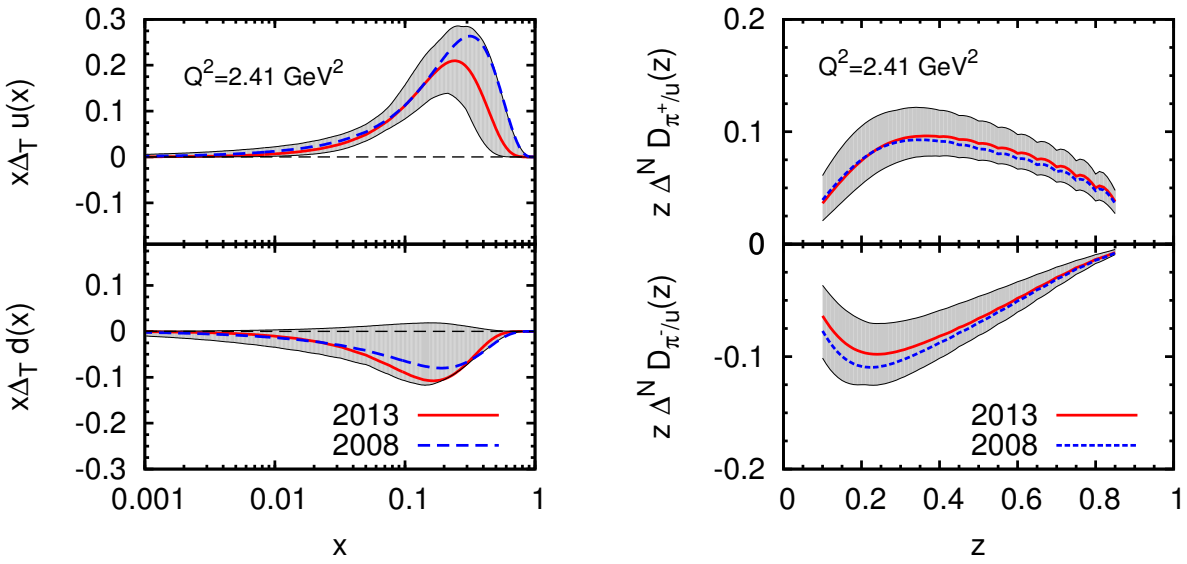

Figure 3.8: The quark transversity (left) distributions, and the Collins fragmentation functions (right) as extracted from SIDIS and BELLE e^+e^- data [61]. In both cases the solid red curve indicates the distributions as determined by the global best fit to the data. The gray bands are an indication of the uncertainty in the extraction. In the left panel, the extracted transversity distribution functions $xh_{1q}(x) = x\Delta_T q(x)$ for $q = u, d$ (solid red line) are compared with an earlier fit [60]. In the right panel, the first moment of the favored and the unfavored Collins fragmentation functions with the uncertainty bands are compared with an earlier fit [60].

The existence of non-zero Collins fragmentation function allows the extraction of the quark transversity distributions inside the nucleon. Transversity or $\delta q_f(x)$, is one of the three leading order quark distributions which survive the integration of quark transverse momentum. They are: quark momentum distribution $f_q(x)$, helicity distribution $\Delta f_q(x)$ and transversity distribution $\delta q_f(x)$. Quark transversity is a measure of the quark's spin-alignment along the nucleon's transverse spin direction, and it is different from that of helicity distribution since operations of rotations and boosts do not commute. The 0^{th}-moment of transversity, $\sum_f \int_0^1 \delta q_f(x)dx$, yields nucleon's tensor-charge as one of the fundamental properties of the nucleon just like its charge and magnetic moment. Transversity requires a helicity change of 1-unit between the initial and the final state of the parton such that gluons, which have spin-1, are not allowed to have transversity. Therefore, quark transversity distribution is sensitive only to the valence quark spin structure, and its Q^2 evolution follows that of non-singlet densities which do not couple with any gluon related quantities, a completely different behavior compared to that of the longitudinal spin structure. These attributes provide an important test of our understanding of the anti-quark and gluon longitudinal spin structure functions, especially with regard to relativistic effects.

3.2.8 Quark Sivers distribution extracted from global fit of SIDIS data

The "Sivers effect", and the quark Sivers distributions as a completely different mechanism, was thought to be forbidden since early 1990s due to its odd nature under the "naive" time-reversal operation. It was only in 2002 when Brodsky *et al.* [62] demonstrated that when quark's transverse motion is considered a left-right biased quark Sivers distribution is not only allowed, it could also be large enough to account for the large observed inclusive hadron SSAs in $p+p$ collisions. Subsequent SIDIS measurements have shown the existence of such non-zero Sivers SSAs in HERMES and COMPASS proton target data.

Since the Sivers SSA is related to the convolution products of the quark Sivers distributions $f_{1T}^{\perp}$ and the "regular-type" spin-independent quark to hadron fragmentation function, which are reasonably well-known through e^+e^- annihilation and SIDIS hadron production data, quark Sivers distributions have been extracted through global QCD fits [63] of existing proton and deuteron targets SIDIS data, as shown in Fig. 3.9. An illustration of quark 2D density distribution from a Lattice-QCD calculation is also shown, indicating a left-right imbalance of quark density in a transversely polarized nucleon. Sivers function $f_{1T}^{\perp}$ represents a correlation between the nucleon spin and the quark transverse momentum, and it corresponds to the imaginary part of the interference between light-cone wave function components differing by one unit of orbital angular momentum [62]. A nonzero $f_{1T}^{\perp}$ arises due to initial (ISI) and/or final-state interactions (FSI) between the struck parton and the remnant of the polarized nucleon [62]. It was further demonstrated through gauge invariance that the same Sivers function, originates from a gauge link, would lead to SSAs in SIDIS from FSI and in Drell-Yan from ISI but with an opposite sign [**?**, **?**]. This "modified universality" of quark Sivers distribution is an important test of the QCD gauge-link formalism, and the underline assumption of QCD factorization used to calculate these initial/final state colored interactions. A direct test of such a fundamental QCD prediction of Sivers function sign change between SIDIS and Drell-Yan has become a major challenge to spin physics, and it has been designated an DOE/NSAC milestone. Polarized Drell-Yan experiments are currently under preparation at COMPASS, and more recently, two experiments with either polarized beam (P-1027) and polarized target (P-1039) have been approved at Fermilab to measure SSA in fixed target Drell-Yan reactions. The ex-

istence of non-zero quark Sivers distributions is now generally accepted and well defined. Quark Sivers distribution provides an interesting window into the transverse structure of the nucleon, and provides constraints to quark's orbital angular momentum, although currently only in a model-dependent fashion. For example, using a lattice-QCD "inspired" assumption that links quark Sivers distribution with quark Generalized Parton Distributions E, quark total angular momentum (J^q) has been quantified [64] for the first time as: $J^u = 0.266 \pm 0.002^{+0.009}_{-0.014}$ and $J^d = -0.012 \pm 0.003^{+0.024}_{-0.006}$.

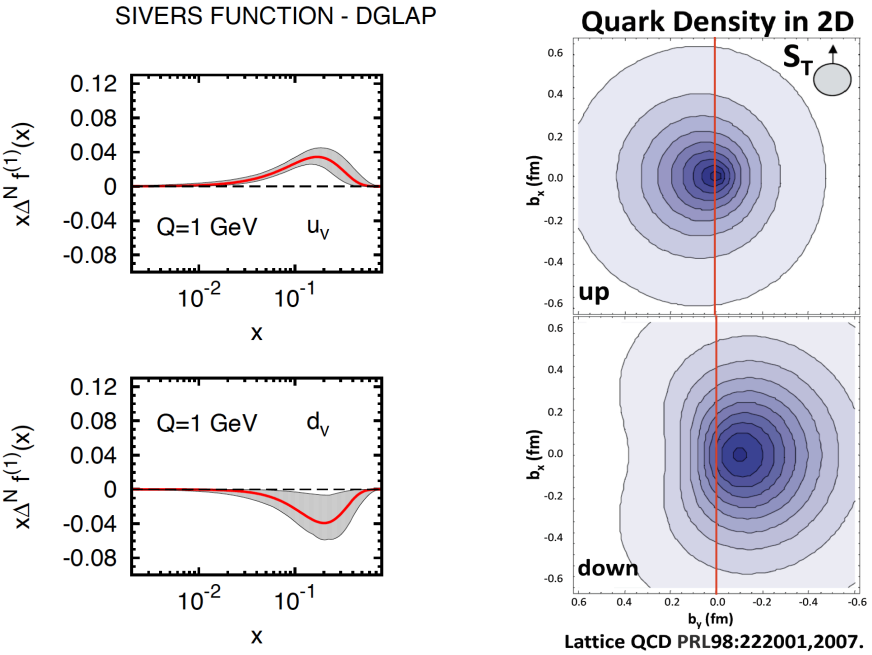

Figure 3.9: The quark Sivers distributions (left plot), as extracted from published proton and deuteron target SIDIS data, for up-quark (top) and down-quark (bottom). The gray bands are an indication of the uncertainty in the extraction. A Lattice-QCD calculation of quark 2-dimensional density distribution in the impact parameter space (b_x vs b_y) for up-quark and down-quark is shown (right plot) with the nucleon polarized in the transverse direction.

Linking the Sivers effect with the twist-3 colinear factorization approach, the twist-3 transverse-spin-dependent quark-gluon correlation function $T_{q,F}(x,x)$ extracted from $p+p$ inclusive SSA data was shown to be directly related to the moments of Sivers functions, thus provide an independent check of our understanding of SSA phenomena in SIDIS and in $p+p$. However, very recent studies by Kang et al. showed that **the quark Sivers function moments extracted by these two methods are similar in size, but opposite in sign** [65], as shown in Figure 3.10 for the up-quark (left) and the down-quark (right). The solid lines represent twist-3 approach "direct extraction" from $p+p$ inclusive SSA data, while the dashed and dotted lines represent Sivers functions extracted from published SIDIS data assuming two different functional forms. This controversy of Sivers function sign "mismatch" indicates either a serious flaw in our understanding of transverse spin phenomena, or alternatively drastic behaviors [66] of quark Sivers function in high momentum fraction (x) or in high transverse momentum (k_t). Given the facts that the existing SIDIS measurements are limited to $x \leq 0.35$, high precision $p+p$ SSA measurements at very forward rapidity are urgently needed to provide constraints in the high-x region.

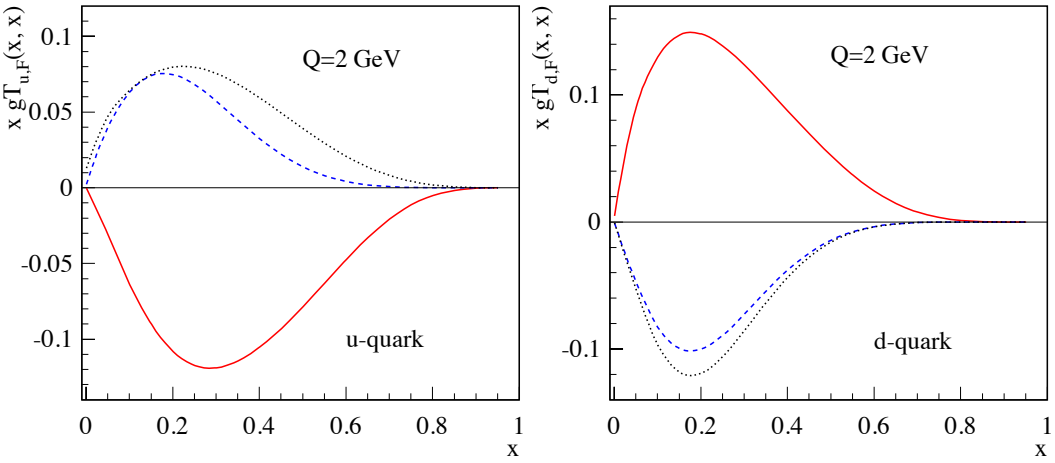

Figure 3.10: The quark-gluon correlation function $gT_{q,F}(x,x)$ as a function of momentum fraction x for u-quarks (left) and d-quarks (right). The solid lines represent "direct extraction" from p+p inclusive SSA data in the twist-3 approach, while the dashed and dotted lines represent Sivers functions extracted from SIDIS data assuming two different functional forms.

3.3 Opportunities for fsPHENIX on Transverse Spin Physics

Unlike polarized SIDIS reactions, existing data of SSA effects in inclusive hadron production in transversely polarized $p+p$ collisions are somewhat more complicated to interpret since both the final state fragmentation effect and the initial state parton distribution effect exist.

(P. Mulders 2013:) It is more challenging, more complicated in terms of the underline QCD color flow. At the same time, the p+p process is much more interesting in understanding the fundamental QCD interactions of quarks and gluons.

From past observations, the single-spin effects in $p+p$ are typically larger than those of SIDIS, thus are much easier for experiments to measure. The main goal of these types of $p+p$ measurements must be to clearly isolate individual effects in SSAs in order to gain a deeper understanding of the fundamental physics.

The detailed comparison between DIS and p+p data, and the possible inconsistencies and controversies within the same theoretical framework, provides the discovery potential of fsPHENIX.

The fsPHENIX, with forward jet and charged hadron capabilities in Stage-I, and with prompt photon, identified hadron and Drell-Yan capabilities in Stage-II will allow a series of transverse spin measurements to be carried out. Especially, the following types of SSA observables are of particular interests due to the fact that a clear separation of Collins and Sivers effects can be achieved in these observables:

3.3.1 Single-Spin Asymmetry of Inclusive Jet (A_N^{jet})

The single-spin asymmetry of inclusive jet (A_N^{jet}) arises purely from the Sivers effect. Since the whole jet is observed in the final state, the quark transverse spin dependent fragmentation function is not involved, therefore, the Collins effect does not contribute to A_N^{jet} as it cancel out in the integration over the azimuthal angle of hadrons inside the jet. A measurement of A_N^{jet} will provide information on the convolution of quark Sivers distributions and the well-known spin-independent fragmentation functions. Predictions of A_N^{jet} in

the fsPHENIX acceptance are at a few % level with a large range of variations reflecting our lack of knowledge on quark Sivers functions at high-x, as shown in Figure 3.13. The measurement of A_N^{jet} can be carried out with the fsPHENIX by recording the jet yields for the different transverse proton spin orientations and constructing the relative luminosity corrected asymmetries between the yields for the up versus down in-coming proton beam's spin orientations.

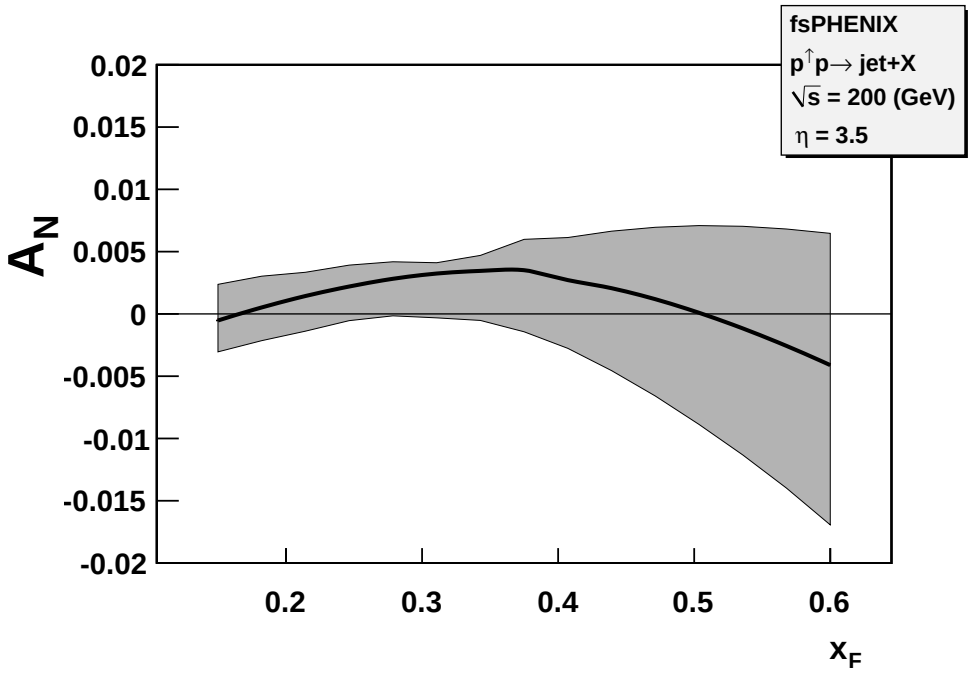

Figure 3.11: The SSAs for inclusive jet production A_N^{jet} in $p^{\uparrow}p$ collisions [52] at $\sqrt{S} = 200$ GeV, as functions of x_F for rapidity $y = 3.5$.

3.3.2 Charged hadron tagged jet single-spin asymmetry A_N^{T-jet}

. Which is purely sensitive to quark Sivers distributions, but with different combination effects from u-quark and d-quark. Following Field and Feynman [67] we define a weighted-jet charge Q as:

Relatively speaking, positively Q-charge jets contain more contributions from u-quark, while negatively Q-charge jets contains more contributions from d-quarks.

3.3.3 Charged hadron azimuthal distribution asymmetry inside a jet (A_N^{h-jet}) arises purely from the Collins effect.

The quark's transverse spin (transversity) can generate a left-right bias inside a jet. A measurement of A_N^{h-jet} will provide constraints on the product of quark transversity distributions and the Collins fragmentation function. Specifically for fsPHENIX, the azimuthal asymmetry of charged hadron inside a jet (A_N^{h-jet}) is a pure Collins effect. The experimental observable in fsPHENIX would be the azimuthal distribution of charged hadron yields around the jet axis reconstructed with the fsPHENIX, and the azimuthal angle ϕ_S is between the proton spin direction $\vec{S}_p$ and the transverse momentum $\vec{k}_T$ of the hadron with

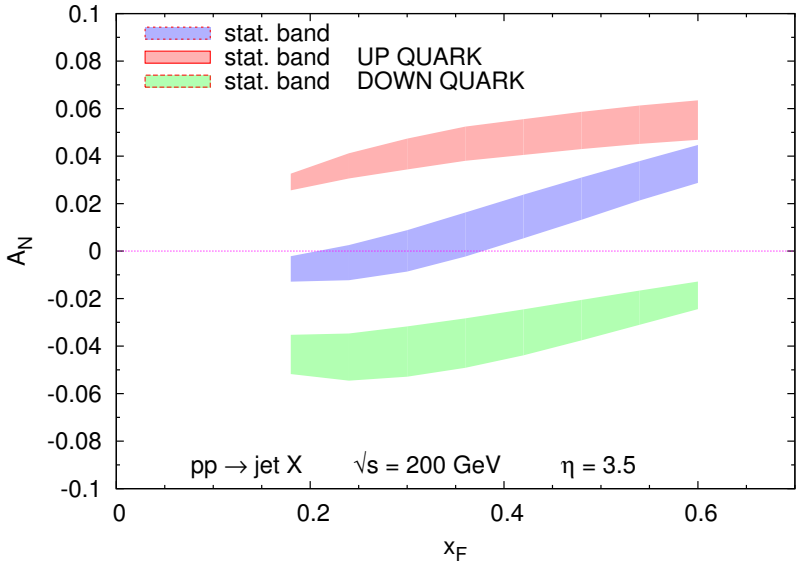

Figure 3.12: The SSAs for inclusive jet production A_N^{jet} in $p^{\uparrow}p$ collisions [52] at $\sqrt{S} = 200$ GeV, as functions of x_F for rapidity $y = 3.5$.

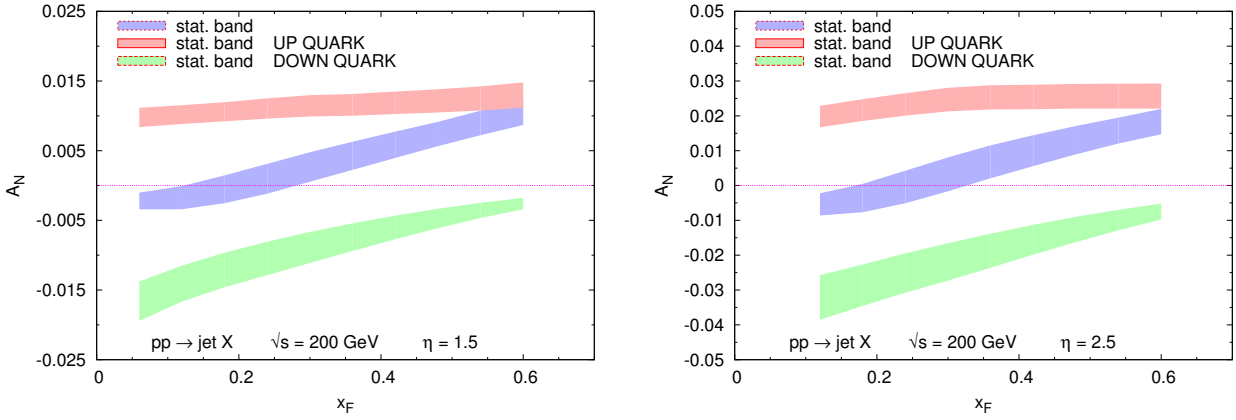

Figure 3.13: The SSAs for inclusive jet production A_N^{jet} in $p^{\uparrow}p$ collisions [52] at $\sqrt{S} = 200$ GeV, as functions of x_F for rapidity $y = 1.5$ (left) and $y = 2.5$ (right).

respect to the jet axis, $\vec{p}_{jet}$ One advantage that such a measurement would have over existing SIDIS measurements would be that the x range measured for the transversity distribution would be substantially higher than that reached in SIDIS, such as at JLab-12 GeV.

The hadron azimuthal distribution asymmetry [40] in Section 3.2.2 A_N can be defined as

$$A_N = \frac{\int dy_2 \sum_{qb} x' f_b(x') x \delta q_T(x) \delta\hat{q}^{(1/2)}(z_h) H^{\text{Collins}}_{qb\to qb}}{\int dy_2 \sum_{abc} x' f_b(x') x f_a(x) D^h_c(z_h) H^{\text{UU}}_{ab\to cd}} \ , \tag{3.2}$$

where $\delta\hat{q}^{(1/2)}(z_h)$ is the so-called 1/2-moment of the Collins function,

$$\delta\hat{q}^{(1/2)}(z_h) = \int d^2 P_{hT} \frac{|P_{hT}|}{M_h} \delta\hat{q}(z_h, P_{hT}) \ . \tag{3.3}$$

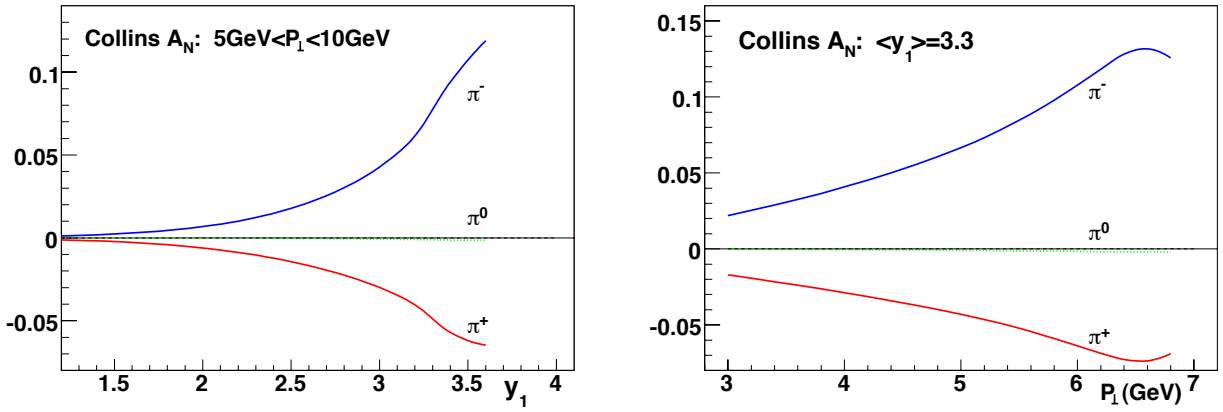

Figure 3.14: Predictions of Collins SSAs for pions in a jet in pp collision at $\sqrt{s} = 200GeV$ at RHIC [40]: left panel as functions of the jet rapidity y_1; right panel as functions of the jet transverse momentum $P_\perp$.

The most critical experimental performance parameters for these type of fsPHENIX measurements would include the angular resolution for the direction of the jet axis and the resolution in the hadron momentum fraction z. Uncertainties in knowing the jet axis will dilute the amplitude of the azimuthal Collins asymmetry and uncertainties in measuring hadron's energy fraction ($z = E_h/E_{jet}$) will smear the spin analyzing power of the Collins fragmentation function in the stage of data interpretation. The latter of these two is very important, given that the Collins fragmentation function has a strong z-dependence, see Figure 3.8.

3.3.4 Di-hadron correlated azimuthal distribution asymmetry (A_N^{2h}) arises purely from the Collins effect.

Which is purely sensitive to quark transversity distributions coupled to the chiral-odd di-hadron interference fragmentation functions (IFF).

3.3.5 Transverse Λ (and $\bar{\Lambda}$) final state polarization in $p^\uparrow + p \to \Lambda^\uparrow(\bar{\Lambda}^\uparrow) + X$

Which is purely sensitive to quark (or anti-quark) transversity coupled with spin-transfer fragmentation functions which can be accessed through e^+e^- data. Although the chiral-odd spin transfer fragmentation function is not well constrained yet by experimental data,

positivity bounds were introduced [68] to estimate the limit of $p^{\uparrow} + p \to \Lambda^{\uparrow} + X$ transverse spin transfer D_{NN}, as shown in Fig. 3.15 for $\sqrt{s} = 500$ GeV. An updated theory prediction of D_{NN} for $\sqrt{s} = 200$ and 500 GeV will be available soon.

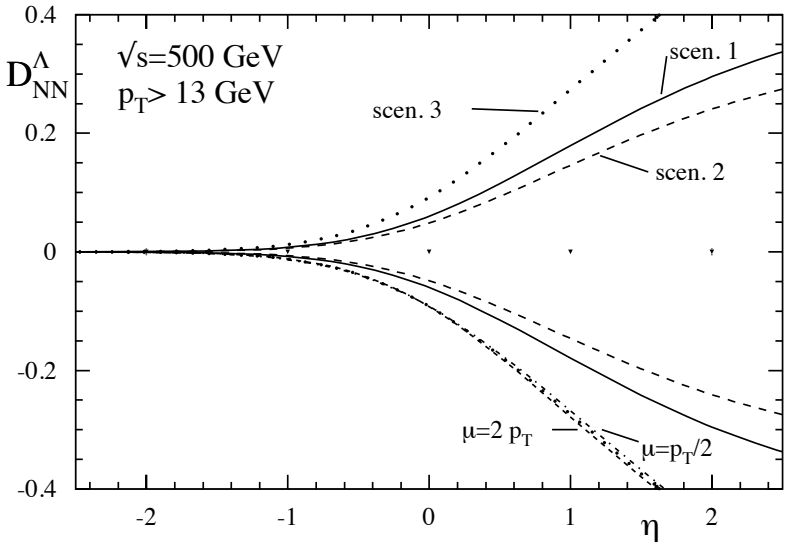

Figure 3.15: The estimated bounds [68] on $p^{\uparrow} + p \to \Lambda^{\uparrow} + X$ transverse spin transfer D_{NN} for $\sqrt{s} = 500$ GeV.

3.3.6 Measurements Simulated

3.3.7 Expected results on transverse spin for fsPHENIX

Chapter 4

Studies of The Properties of Nucleus through p+A Collisions

4.1 Introduction

By studying the particle productions at p+A collisions, we can understand the parton modification and its evolution in the nuclei. There are several probes to study the collision matter, and quarkonia production is a good probe to explore the gluon distribution of the nucleon since quarkonia are produced dominantly by the gluon-gluon fusion process in high-energy collisions [69, 70]. Recently, the PHENIX collaboration has reported J/ψ suppression in $\sqrt{s_{NN}} = 200$ GeV deuteron-gold (d+Au) collisions at the Relativistic Heavy Ion Collider [71]. And the centrality dependence of these J/ψ suppression results at forward rapidity is not well described quantitatively by nuclear shadowing models that include final-state breakup effects [72]. By fsPHENIX detectors, we expect to reach smaller x region upto $1*10^{-3}$ and get better understanding on shadowing and saturation scale [73, 74].

As another probe, Drell-Yan di-lepton production provides valuable information about the partonic structure of hadrons that is complementary to deep-inelastic scattering (DIS) studies because it distinguishes between quarks and antiquarks. Specially for p+A collision, Drell-Yan process gives clean signal to study the initial state effects of shadowing and parton energy loss since the decay di-lepton in the final state does not interact strongly with the partons in the medium. The Drell-Yan measurements at lower center-of-mass energy [75] indicates that the forward rapidity at $\sqrt{s_{NN}} = 200$ GeV would reach into the parton shadowing region, but the region at this energy is not explored yet. Thus the Drell-Yan production at forward rapidity will be the key measurement to understand the mechanism of the initial states effects between the shadowing and the parton energy loss.

4.2 Estimation on the significance of signal

4.2.1 Luminosity, cross section & signal

Figure 4.1 shows differential Drell-Yan cross section vs. mass. The collected number of Drell-Yan events can be estimated with the integrated luminosity and Drell-Yan cross section. The equation below shows the relation and the number of Drell-Yan events we would collect with the assumed luminosity.

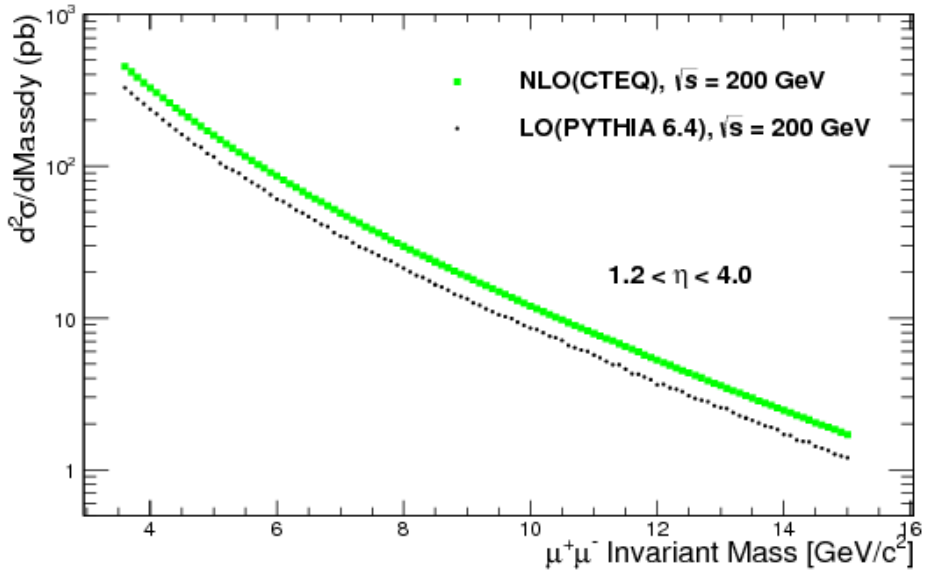

Figure 4.1: (color online) Drell-Yan cross section vs mass of a PYTHIA calculation [76] and NLO calculation [77]

.

$$\frac{d\sigma_{\rm DY}}{dm} \cdot \mathcal{L} \cdot \epsilon_{\rm DY}^{\rm BBC} \cdot A\epsilon_{\rm DY} = \frac{N_{\rm DY}}{\Delta m}, \tag{4.1}$$

where, $\frac{d\sigma_{\rm DY}}{dm}$ is the differential cross section of the Drell-Yan process, $q\bar{q} \rightarrow \gamma^* \rightarrow \mu^+\mu^-$ from the NLO calculation for each mass bin in the pseudorapidity region, $1.2 < |\eta| < 4.0$. $\mathcal{L}$ stands for the integrated luminosity. $\epsilon_{\rm DY}^{\rm BBC}$ is the BBC efficiency of hard process which contains a muon pair from Drell-Yan process. And $A\epsilon_{\rm DY}$ is acceptance and efficiency correction for the Drell-Yan pair. At RHS, $\frac{N_{\rm DY}}{\Delta m}$ is the Drell-Yan pairs which we would collect for the mass bin.

NLO calculation provides the integrated cross section of 258 pb for the mass region from 4 GeV to 8 GeV. And we expect to collect the integrated luminosity, $\mathcal{L}$ of 100 pb^{-1}. So assuming the efficiencies, $\epsilon_{\rm DY}^{\rm BBC} \cdot A\epsilon_{\rm DY}$ as 0.5, we would collect $\frac{d\sigma_{\rm DY}}{dm} \cdot \mathcal{L} \cdot 0.5 = 258pb \cdot 100pb^{\cdot 1} \cdot 0.5 = 12.9\ k$ for the mass bin of 4 GeV to 8 GeV.

4.2.2 Background estimation

The mass region between 4 and 8 GeV (above the J/ψ, ψ' masses and below the Υ mass) is dominated by the Drell-Yan process, correlated open-heavy flavor decays, light hadrons and its decays. And we expect to distinguish each process using they have different decay lengthes each other. Drell-Yan process is promptly produced from the collision point, whereas leptons from open-heavy flavors are produced by semi-leptonic decay having decay length of $\sim$200μm. Moreover, light hadrons have huge decay lengh over few meters. Thus, measuring the displaced vertices using the silicon vertex detector will be the powerful tool to discriminate Drell-Yan production from open-heavy correlated and hadron decay backgrounds. Assuming the $c\bar{c}$ and $b\bar{b}$ cross sections measured at PHENIX and

STAR [78, 79, 80, 81], the yields of Drell-Yan process and correlated open-heavy flavor pairs would be about the same within the experimental uncertainty. And the hadron background would be a certain amount in case that it can not be distingushed from the normal lepton tracks. Considering those backgrounds, the S/B ratio can be assumed as 1/3 as a fair amount.

4.2.3 Yields

To measure the nuclear effects in p+Au collision, we use nuclear modification factor, $R_{p\mathrm{Au}}$, which is the relative yield of p+Au collision to p+p collision when it is scaled by the number of binary collision. And it is defiend as

$$R_{p\mathrm{Au}} = \frac{dN_{\mathrm{DY}}^{p\mathrm{Au}}/dm}{\langle N_{\mathrm{coll}}\rangle\, dN_{\mathrm{DY}}^{pp}/dm}, \tag{4.2}$$

For the modification factor, we can estimate the statistical uncertainties with the levels of the statistics of the signal and the backgrounds, which are discussed at the previous section 4.2.1, 4.2.2. Explicitly, the statistical uncertainty for each bin is defined as

$$\text{S. U. } of\ R_{p\mathrm{Au}} = R_{p\mathrm{Au}} \times \sqrt{(\frac{\text{S. U. in } pp}{N_{\mathrm{DY}}^{pp}})^2 + (\frac{\text{S .U. in } p\mathrm{Au}}{N_{\mathrm{DY}}^{p\mathrm{Au}}})^2}, \tag{4.3}$$

where statistical uncertainties, S.U. in pp or in pAu are estimated by square-root of the total events including the signal and the backgrounds to consider the background contamination.

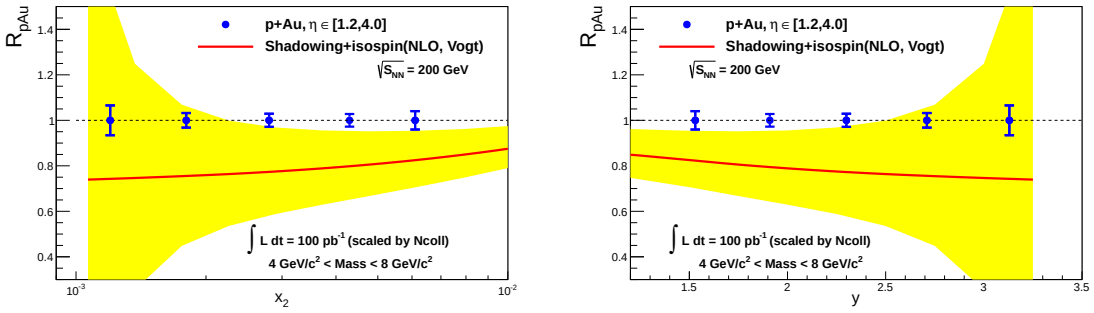

Figure 4.2: (color online) $R_{p\mathrm{Au}}$ vs x(top pannel) and rapidity(bottom pannel) for Drell-Yan process. Blue points show the estimation with statistical uncertainties by fsPHENIX. Red curves are from NLO shadowing caculation and yellow shaded bands are theoretical uncertainty on the $R_{p\mathrm{Au}}$

.

Figure 4.2 shows $R_{p\mathrm{Au}}$ measurement and the uncertainty for the Drell-Yan process with fsPHENIX detector. The theory estimation is from NLO shadowing calculation considering isospin effects and shows ~20% suppression at most small x region and the most forward rapidity region. The statistical uncertainties for the measurement are estimated as between 2% and 4% depeding on each bin's statistics. And this amount of sensitivity will give significant constratints to the shadowing model given the large suppression level from the theory. Fig. 4.3 shows J/ψ $R_{p\mathrm{Au}}$ projection onto NLO EPS shadowing model [73]. And we see that fsPHENIX samples much smaller x than the region which current PHENIX

forward detector can reach to. These very forward points will give valuable information to understand the saturation region [74] with combination of the final state breakup effect [82].

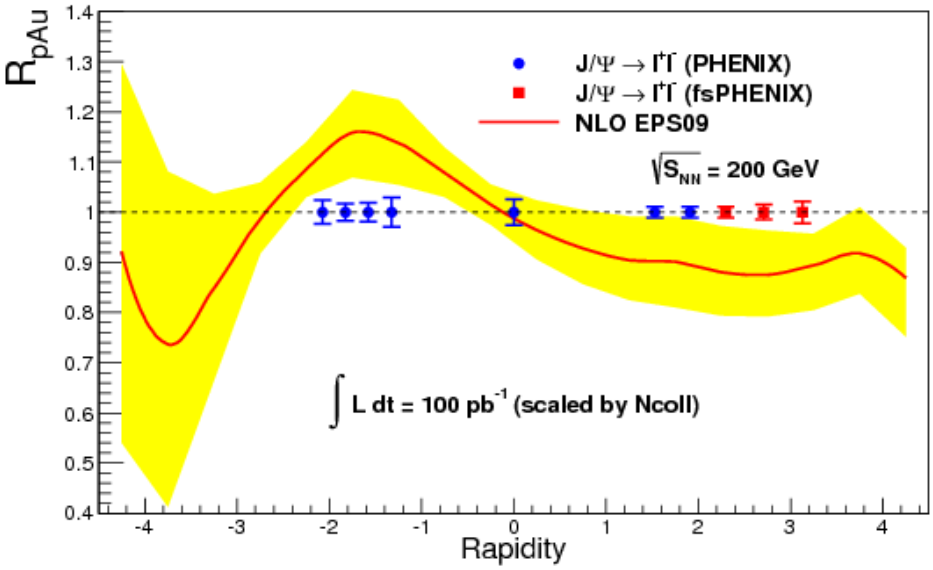

Figure 4.3: (color online) J/ψ $R_{p\mathrm{Au}}$ vs rapidity. Blue points are region covered by current PHENIX detector and red points are by fsPHENIX upgrade. Red curves are from NLO shadowing caculation and yellow shaded bands are theoretical uncertainty on the $R_{p\mathrm{Au}}$

.

Chapter 5

Properties of Quark Gluon Plasma in Heavy Ion Collisions

Chapter 6

The fsPHENIX Detector Designs and Challenges

6.1 Detector Design

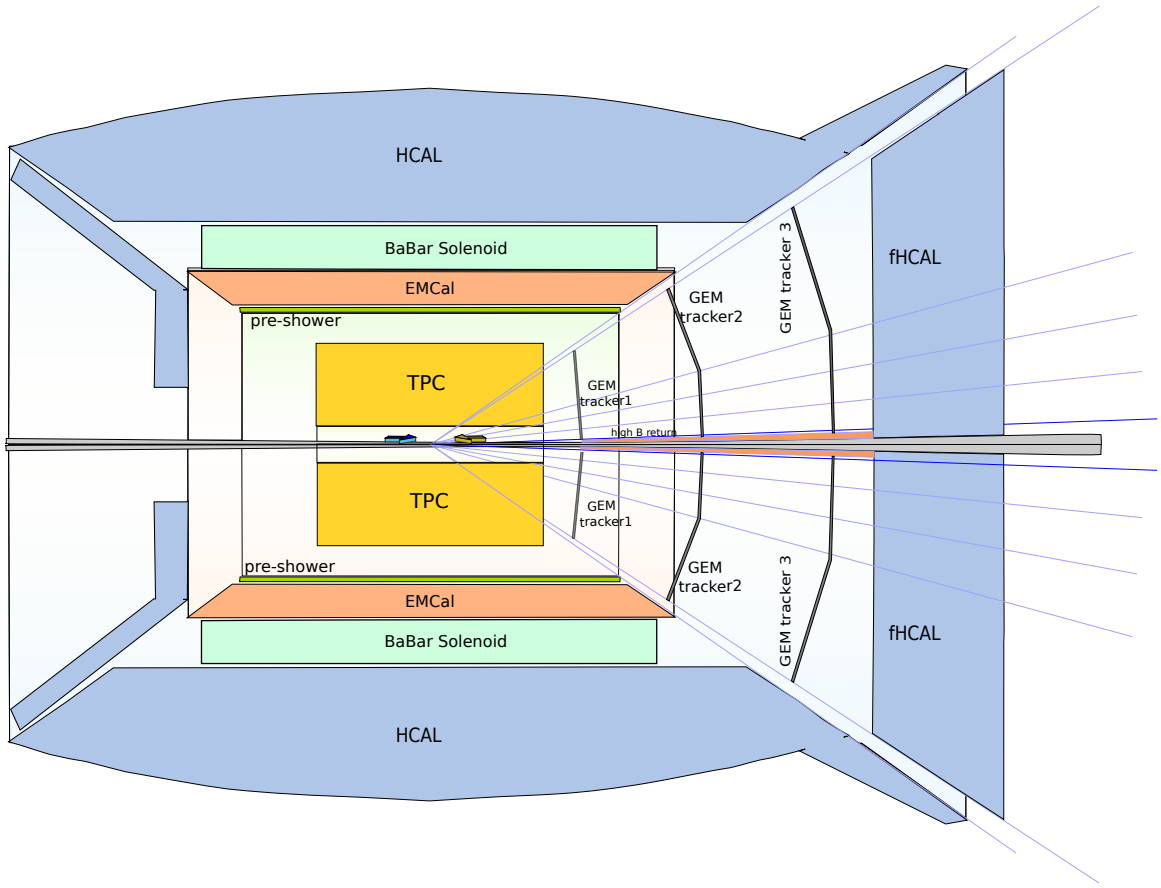

Figure 6.1: Overview sPHENIX design including the fsPHENIX.

In this section we describe the general idea of the forward sPHENIX detector system with some details about geometry, readout and some cost estimations.

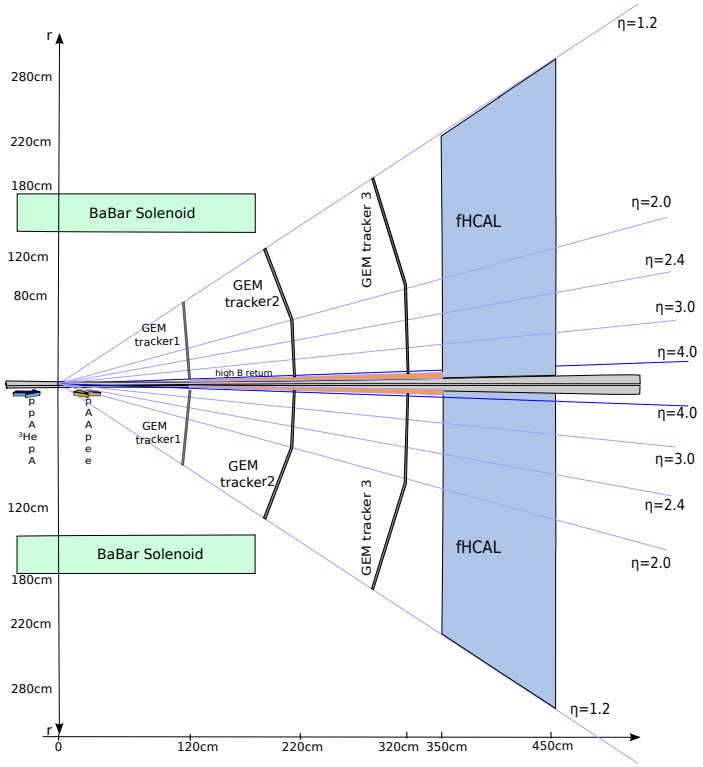

Figure 6.2: Overview of the forward part of the sPHENIX.

The overview of the sPHENIX can be found in Figure 6.1. It contain most of the hadron side ePHENIX detectors planed to take place during the eRHIC era. A detail of the forward part (fsPHENIX) is shown in Figure 6.2. The detector is designed to cover the rapidity $\eta \in [1.2, 4.1]$. The rapidity gap between the barrel sPHENIX and fsPHENIX $\in [1.0, 1.2]$ is thought to be the space for electronic cables and the magnet cryogenics machinery. The smallest angle is 2 degrees and is limited by the beam pipe and the magnetic piston. The fsPHENIX is in the direction of the protons in p+A collisions. At the smallest angle the Björken x scanned for pions is $2 \times 10^{-}4$.

In the ePHENIX phase of the detector, it will work as the hadron going detector. The changes needed for ePHENIX includes a Cerenkov detector which will take place between GEM tracker station 2 and 3 in Figure 6.2.

The entire fsPHENIX detector is comprise up to 460cm away from the interaction point. Beyond this point, a eRHIC combined magnet will take place according to the current thinking of the eRHIC design. If this combined magnet is moved forward, the luminosities will reduce by a factor of Z^2 [NEED REFERENCE].

In the next subsections we detail all the active and passive peaces of the detector.

6.1.1 Beam Pipe

The design considered the current beryllium beam pipe geometry. It has a radius of 2 cm at Z =0 and 5 cm at Z =500 cm. One important consideration for these dimension is that particles with pseudo-rapidity $\eta \sim 4$ will emerge from the beam pipe only after 40 cm.

6.1.2 Magnetic System

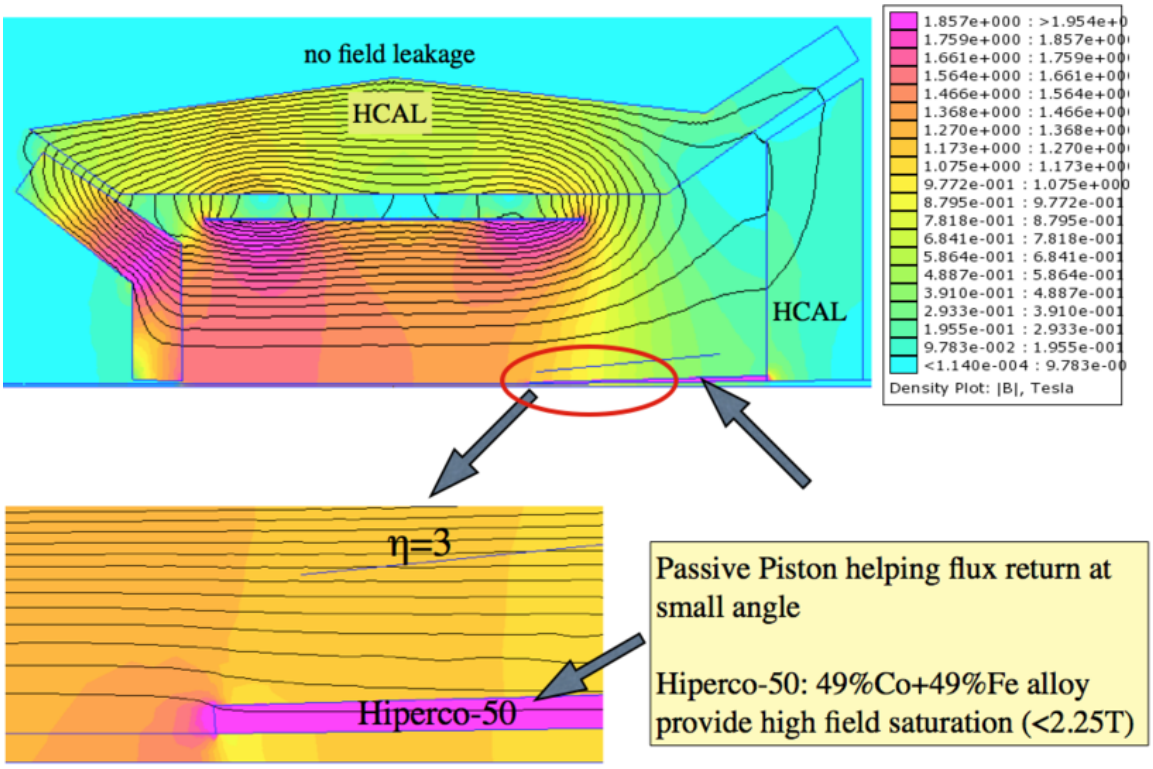

Figure 6.3: Magnet system for sPHENIX.

Probably the most discussed part of the fsPHENIX design was the magnetic system. The magnetic field needs to be enough to measure dileptons from Drell-Yan at *eta* up to 4, or something about $\delta p/p = 0.002p$.

A natural choice would be a dipole, which provide the maximum analyzing power for momentum measurement. The problem in use dipoles in fsPHENIX is the large interference with the beam line. Detectors like ALICE and LHCb at LHC have dipoles in their forward directions but the beam has energy 13 times larger than RHIC and the magnetic field strength of these dipoles don't interfere significantly with the bem. Some ideas have been studied to magnetically shield the beam pipe to solve this problem, however, another issues can emerge from a dipole design even in the case when the beam can be shielded. Because of the space limitation, a dipole needs to be close to the barrel solenoid, making a coupling between these two devices very challenging. Another problems include the acceptance lose for the cryogenic system for the beam shielding and the unpredicted behavior of the radiation from electron beam in the eRHIC phase. Other possibilities were explored like a toroid, with serious implications for the detector acceptance, and additional bucking field solenoids, which a large cost and mechanical challenges when close to the barrel solenoid.

The acquisition of the BaBar magnetic by PHENIX was a game changer for fsPHENIX magnetic design. The BaBar magnet is a 1.5 Tesla superconducting solenoid with extension of 3.7m and 1.4 m radius [Nucl.Phys.B78, 559 (1999)]. The solenoid has three longitudinal segments with larger number of turns in the edges of the solenoid. This configuration makes the magnetic field more uniform throughout the solenoid extension, a big advantage

for forward physics since it enhance the fringe field at the edges.

We used the free software FEMM 2D and Poisson in order to produce the field map for fsPHENIX simulations. We assumed radial symmetry in these 2D simulators which is a very reasonable assumption for a solenoid and symmetric detectors. Figure 6.3-top shows the field lines and strength result for this magnet coupled with the magnetic material of the rest of the detector. The hadronic calorimeter (HCal) was considered to be made purely from stainless steel. Neither materials reach a magnetic field density close to saturation, hence a more detailed study considering the scintillator volume of these detectors was necessary. A return yoke of stainless steel was added at $Z \sim$ -2m to keep the entire detector magnetically hermetic. No field leakage is observed on these simulations.

The momentum measurement is proportional to $\vec{B_T} \times \vec{p}$. The transverse component of the field B_T gets rapidly weaker for η >2.5. Changes in the current densities between the solenoid sectors does not change this picture. The needed B_T at small angles can be obtained from a distrotion of the field line in a small region close to the beam pipe.

The solution proposed is a passive magnetic material piston surrounding the beam pipe. The magnetic material must have a large saturation point. Alloys with a large cobalt concentration are known to allow a high saturation point. One of these materials is the copyrighted named HIPERCO-50 with a 49%Co+49%Fe composition. The internal magnetic field saturates at 2.25 Tesla. The bottom picture in Figure 6.3 shows a zoom in of the field lines next to this piston. The field is distorted by an angle around 2 degrees, similar to the angle between the particles and the beam line. This can roughly improve the momentum resolution by a factor of 2 if a tracker is placed next to the tip of the piston. Figure 6.4 shows the trajectory of particles crossing different η angles. The trajectories are relative to a measurement made by a hypothetical station placed at 30cm for particles with angles $1.2 < \eta < 3.0$ and 60cm for particles with angles $3.0 < \eta < 4.1$. The stations are placed right after the position where all particles come out from the beam pipe. For jet physics, the particles are assumed to be produced at the vertex, that is, the tracking algorithm can use the primary vertex position as measured by the vertex detector for the lever arm tracking.

A first order approximation of the momentum resolution was calculated with the field map generated from FEMM. The calculation assumed a tracker detector with a angular resolution of 0.5 mrad or 50 μm for $\eta > 3$ which is the limitation for GEM tracker technology. Another assumption made in this calculation is the lever arm measurement at 10cm, which demands a track projection based on vertex detectors. Figure 6.5 presents the calculated momentum resolution from these calculations. The calculation confirms that the momentum resolution at very small angles is improved by a factor of 2, limiting the maximum $\delta p/p/p$ of 0.3%.

The solution proposed here does no require any additional field other than the one provided y the BaBar magnet and no active devices. The cost of the HIPERCO-50 material was not quoted yet, but we assume it is not going to drive the cost of the fsPHENIX project. The magnetic piston may produce a large background from particles with $\eta > 4.2$ showering into the piston material. One solution for this problem can be the addition of tungsten teeth surrounding the piston. These teeth can help stop the particle shower from the interior of the piston. This solution was previously used in SPS experiments at CERN [NEED REFERENCE]. A sketch of this idea is shown in Figure 6.6. Further studies concerning the background that this piston can introduce at small angles are the subject of future R&D.

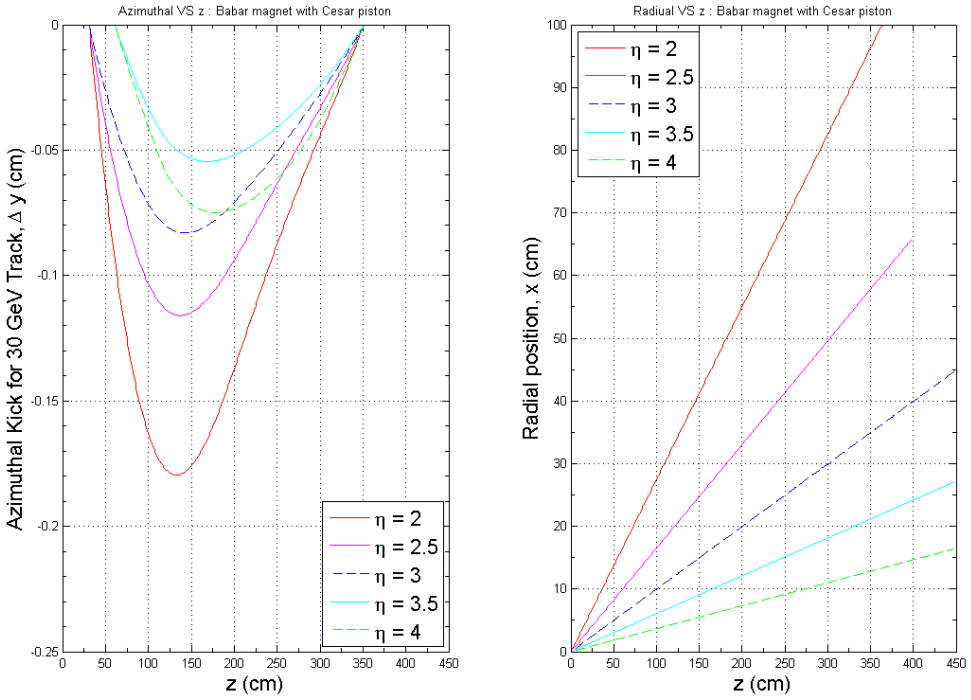

Figure 6.4: Trajectory of a GeV/$c$particle at different η regions, relative to the position measured at 30cm for $1.2 < \eta < 3.0$ and 60cm at $3.0 < \eta < 4.1$.

6.1.3 Tracking System

The tracking requirements for fsPHENIX is mainly to measure the leading particle shift within the jet and its fragmentation and a momentum resolution enough for the future particle identification in eRHIC. Most of the challenges are in the rapidity >2.5.

We mentioned in the last section that the magnet system is not optimized to measure momentum in the forward direction. A good analyzing power may come from a tracking system with a very good angular momentum resolution. More precisely, in order to achieve the momentum resolution of $\delta p/p = 0.2\%p$ shown in Figure 6.5-left, the tracking system may resolve the azimuthal angle in 0.5 mrad at a Z positions 20cm, 125cm and >230cm. The position of the first station also depends on the Z positions where the small angle particles emerge from the bem pipe. At $eta = 4.1$, considering the beam pipe has a radius of 2cm, it happens for $Z = 60$cm. For $\eta = 3.0$ it happens at $Z = 20$cm, confirming this is a good place for the first tracking station. The last station can be anywhere forward 230 cm. This is the position where the Cerenkov detector (RICH) will take place. In fact, the PID detector needs to be sandwiched between two tracking stations for pattern recognition. Therefore, a tracking station at Z =210cm and another at Z =314cm are chosen. In the ePHENIX design, these tracking stations are made in two parts each in order to follow the geometry of the RICH mirrors.

Translating the 0.5mrad angular resolution to position resolutions we obtain the numbers listed in Table 6.1.

Some of the state of the art tracking technologies available in the market are Multi-wire

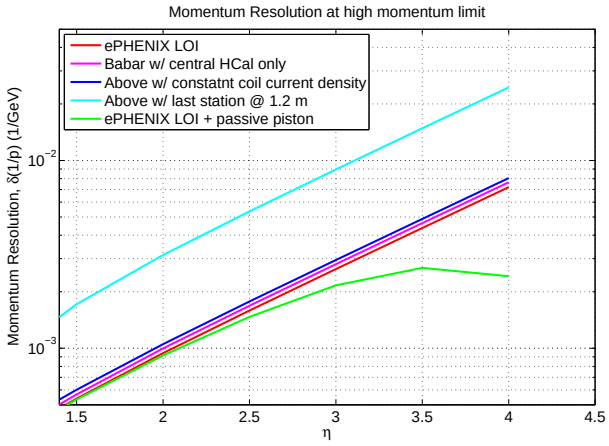

Figure 6.5: Momentum resolution as a function of pseudo-rapidity in different configurations.

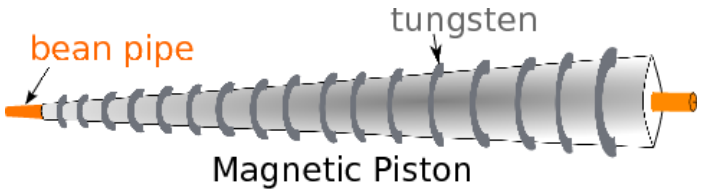

Figure 6.6: Sketch of the magnetic piston evolving the beam pipe and the details of the tungsten teeth to help stop particle showering from the material.

Table 6.1: Position resolutions needed for 0.5 mrad angular resolution.

station Z position	$\eta = 4.1$	$\eta = 3.0$	$\eta = 2.0$	$\eta = 1.2$
20cm	3μm	10μm	28μm	66μm
60cm	10μm	30μm	83μm	199μm
125cm	21μm	62μm	172μm	414μm
314cm	52μm	157μm	433μm	1040μm

proportional chambers with typical position resolutions of 100μm-200μm, micro-omegas, Gas Electron Multipliers (GEM) with resolutions starting from 60 μm [**?**] and silicon detectors with resolutions around 20 μm.

Given the position resolution and the cost, a reasonable choice for the tracking technology is the use of GEM technology for the stations placed at 125cm, 210cm and 320cm. The silicon detector is the only technology which can provide the position resolutions in the tracking stations placed at Z=20cm and Z =60cm. The next sections describe more details of the design of the silicon and GEM stations.

6.1.4 GEM μTPC

The gas electron multiplier technology (GEM) has been extensively used since its invention by Sauli in late nineties [**?**]. The GEM consist of 50 μm kapton coated in both sides of 5μm of copper (Fig. 6.7). This foil contain 70μm holes spaced in 140μm. When a tension of 300-500V is applied between the two copper coats, a strong electrical field of 60-100 kV/cm

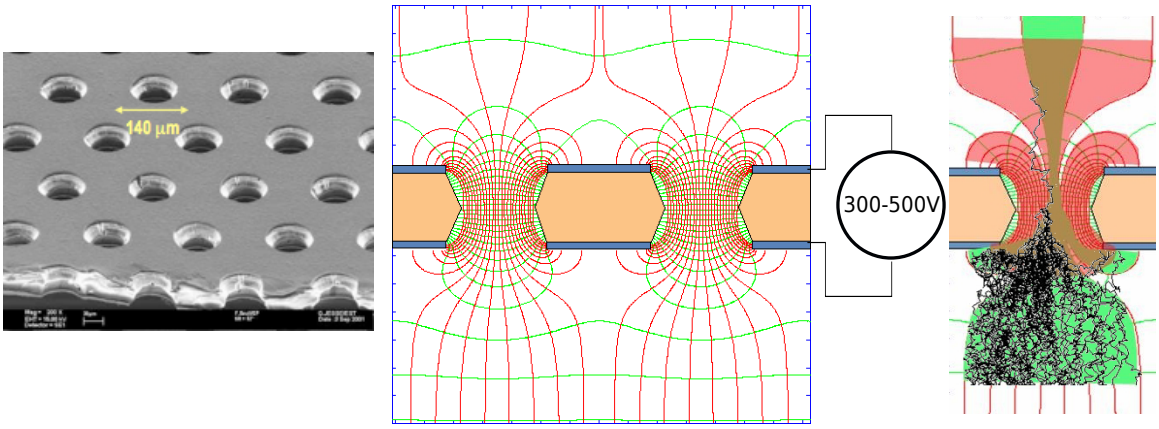

Figure 6.7: Principle of the GEM technology.

appear inside the holes. The GEM foil is placed in a gas volume, usually methane, where secondary electrons are produced from track ionization. When one secondary electrons reach the holes produces an avalanche of 10-20 electrons. Usually, three GEM planes are placed in sequence in order to obtain gas gains of the order of 10^3-10^4.

Table 6.2 lists the dimensions of the GEMs stations in fsPHENIX. GEM etcher in CERN using single sided etch technology can produce 2m $\times$ 0.5m GEM foils [**?**], hence compatible with fsPHENIX needs.

Table 6.2: Dimensions of the GEM stations in fsPHENIX.

Z position	radius [cm]	area [m^2]
125 cm	$4 < r < 73$	1.7
210 cm	$7 < r < 123$	4.7
314 cm	$10 < r < 184$	10.6

One of the best performances when using GEM technology was achieved by COMPASS experiment where 60 μm residuals between track projection and hit was registered using a $X - Y$ readout configuration in a 33 cm^2 area [**?**]. It is a proof of principle the GEMs can provide the position resolutions listed in Table 6.1. In order to obtain 0.5mrad angular resolution we need $0.5\sqrt{12}$ =1.73mrad strips, or 3.6K azimuthal segments. The radial resolution is determined from simulations considering matching parameters between different stations and occupancy. A solution widely used in multi-wire chambers to reduce the number of radial channels is the V configuration where the azimuthal strips form a certain angle. Each readout channel will also provide the time of the hit, providing the Z position of the original ionization inside the chamber. The Z position information improves the tracking recognition of particles coming from interaction point and help in reduce ambiguities in the radial coordinate.

We used GEANT4 hits generated from particle generator events to study the design of the GEM tracker in most though condition in heavy ion collisions and jets in p+p and e+p environments. Most of low level parameters used in this simulation is from other efforts. A future GARFIELD simulation and dedicated test with a real prototype can help to make this simulation more realistic and anticipate future design flaws. We used the design of the Hadron Blind Detector (HBD) seen in Figure 6.8 for the material budget in simulation

[?]. Table 6.3 list the properties of the GEM chamber. Particles from the interaction point should have a momentum of at least 2 GeV/c to overcome the magnetic field in the solenoid and reach the tracking station. These particles may form tracks with small angular variation when crossing the chamber.

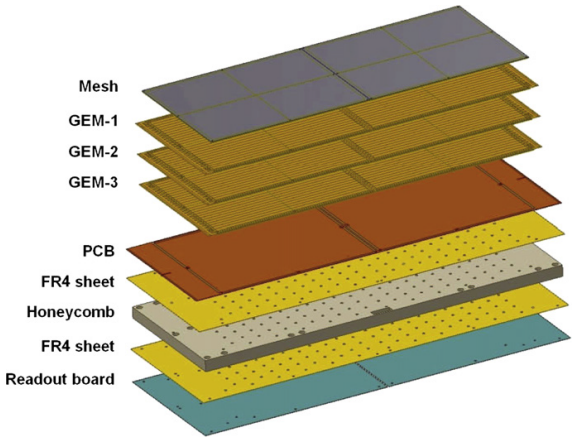

Figure 6.8: GEM station design used in fsPHENIX simulation, similar to HBD [?].

Table 6.3: Material budget and dimensions of the GEM station.

part	material	thickness
window	mylar	100 μm
gas volume	methane	1.4cm
3 GEM planes	copper	5μm
	kapton	50μm
	copper	5μm
induced gap btw. GEM planes	methane	0.15cm
PCB	kapton	50μm
	Copper	5μm
face sheet	G10	250μm
honeycomb		1.905cm
readout board	copper	10μm
chips and sockets	copper	5μm

According to GARFIELD simulations done by third parties [CITATION], the ionization from the crossing particle in the chamber has a diffusion of $\sim 300\mu\text{m}/\sqrt{cm}$. The drift space between the chamber window and the first GEM foil is 1.4cm. We are assuming a drift velocity of 0.3cm/μm, which makes a drift time of ~450 ns.

The hit position is defined by the TDC value of the strip readout and the crossing strips in the V configuration. Each strip crosses

$$N\_crossings = \frac{\theta_{strip}}{\delta\phi} \tag{6.1}$$

$$\delta\phi \quad = \quad \frac{N_{strips}}{2\pi} \tag{6.2}$$

where θ_{strip} is the angle between the top and bottom level strips and N_{strips} is the number of strips in each readout level. For 3.6K azimuthal segments, $N_{strips} = 3.6/2 = 1.8K$ strips in each layer of the readout pad. The top layer is separated by the lower by 50μm of kapton. Given the different efficiencies in collect the charge from the chambers, the bottom layer may be much thicker than the top one. In COMPASS they use 80μm thick strips for the top layer and 350μm for the bottom one.

The number of crossings determine the radial segmentation of the tracker, but it also increases the ambiguity in heavy ion or jet events. The readout may also need to be physically divided radially in few segments to overcome ambiguities; and technical implementations of the strip readout like noise collection and impedance given the length of the strips.

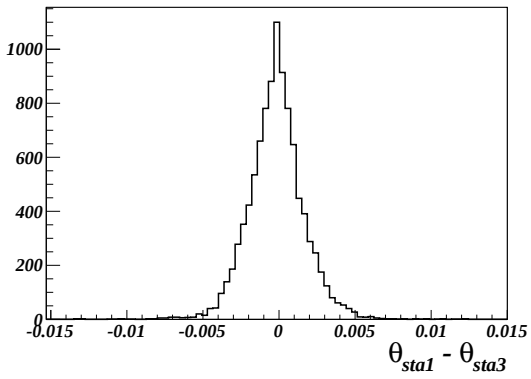

Figure 6.9: Difference between the polar angle of tracks crossing GEM station 1 and station 3 according to thrown pions in GEANT4.

The radial segmentation, or polar angle resolution, required for tracking was determined from simulation and is shown in Figure 6.9. Two tracks can be resolved by the readout in about 5mrad. This range translates to 110 radial segments in the station. According to (6.1), the angle between the strips needed for 110 crossings is $\theta_{strip} = \pi/16$. In order to test for an extreme case where a high multiplicity and area concentrated jet is present, GEANT4 fed with 100 central HIJING events provides an occupancy of 9% for each of the 3.6K strips in the entire pseudo-rapidity range covered by the station. This occupancy is integrated over 5ns sampling, the time resolution of the ionization. For 110 crossings in one strip, ten of them will be fired in one central heavy ion collision or a busy jet event in p+p. This indicates that a radial segmentation larger than 10 is necessary to reduce ambiguity in an extreme event condition. One suggestion is divide the discs in 0.25 units of pseudo-rapidity, or 12 radial segments. An overview of the radial segmentaion of the readout and the orientation of the azimuthal strips is shown in Figure 6.10.

A common issue with tracking is the very poor position resolution for particles incident perpendicularly to the readout plane. Studies performed with a beam test demonstrate that particles with incident start to be measured with a much worse angular resolution for angles smaller than 4 degrees (Fig. 6.11). Particles at $\eta \sim 4$ have an incident angle of 2 degrees. A solution for this problem presented in the fsPHENIX design shown in Figure 6.1 is to tilde the GEM chambers in 3 degrees, escaping from the region with poor resolution.

The chambers may also need to be divided in octants and have a different slope for $\eta > 2$ to fit in the future Cerenkov detector.

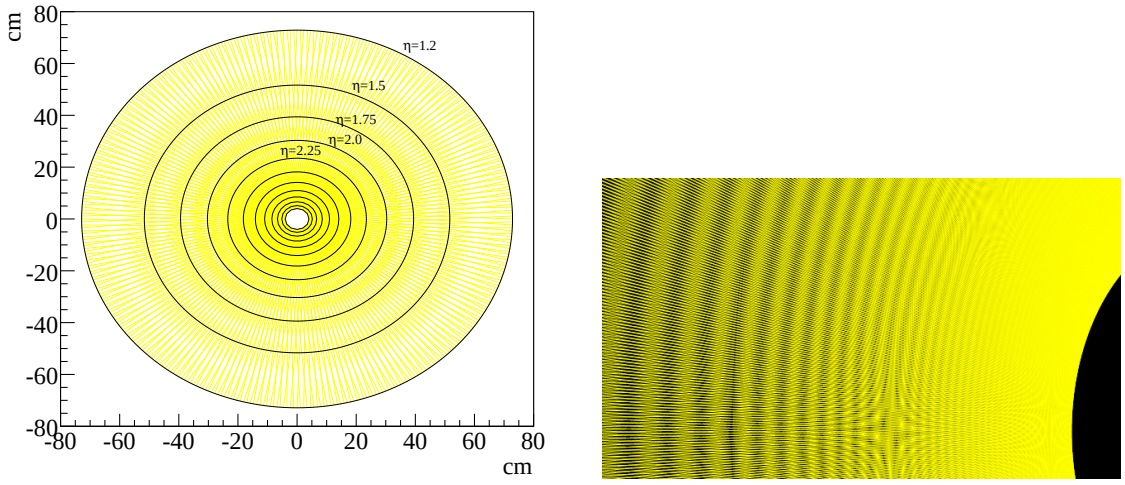

Figure 6.10: (left)Radial segmentation of the GEM readout. Detail of the phi strips (in yellow). Apparent radial segmentation are the points where the strips crosses.

In the current design the readout electronics is based on the VMM1/VMM2 ASIC. A BNL/ATLAS project to develop a chip dedicated to micromegas and time sampling detectors [**?**]. Its 64 channels readout have peak detection and provides 1fC charge and 1ns charge time resolution. The rise time in the pre-amp shaper can be as low as 25ns. The architecture of the ASIC is shown in Figure 6.12. The VMM1 is ready for manufactory but has some limitations like the lack of a digital output and some know bugs. VMM2 is in final design and will be available for manufactory next year.

The cost of each chip is estimated in US$65, or a dollar per channel. According to the current readout design, each GEM station will have 3.6K $\times$ 12=43.2K channels. Other costs which the electronics may incur, like FPGAs, are not estimated by the time of this writing.

6.1.5 Hadronic Calorimeter

In the very preliminary detector simulations we are considering a one meter deep FeSc calorimeter with $4\times4\text{cm}^2$ segmentation. It is composed by 30 layers. Each layer is 4/5 thick iron and 1/5 scintillator. It covers the pseudo-rapidity region $1.2< \eta <5.0$. The iron in the HCAl also works as a field return for the BaBar solenoid.

A more detailed study of the forward HCAL is underway.

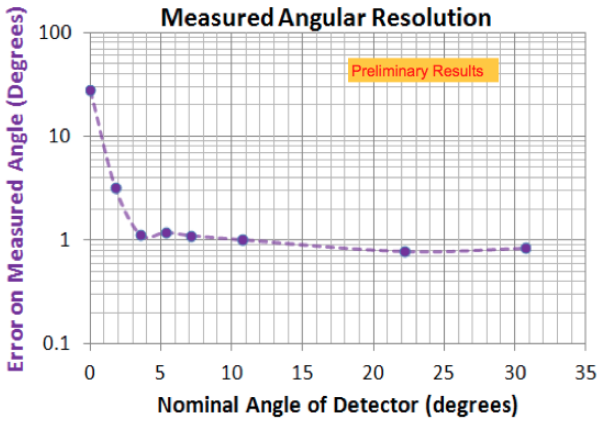

Figure 6.11: Beam incident angle dependence of the angular resolution in the GEM tracker [T.Hemmick,]

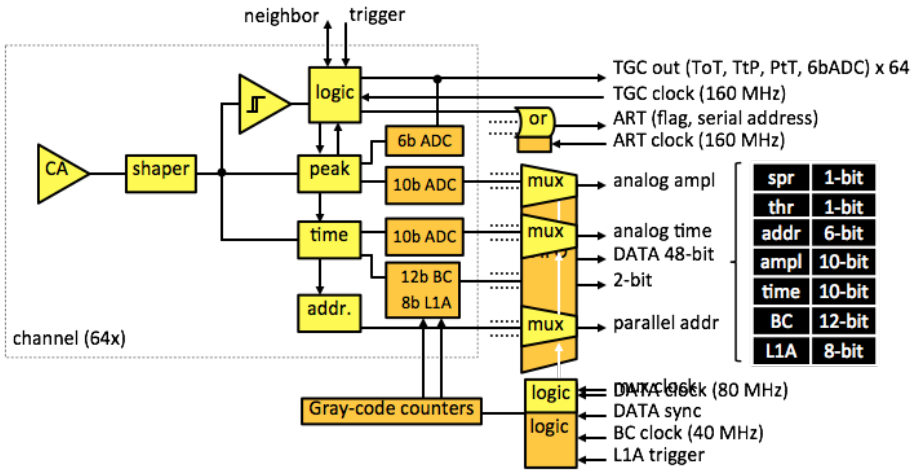

Figure 6.12: Architecture of the VMM2 ASIC suggested to be used in the GEM readout [Gianluigi De Geronimo,BNL - Status Report].

Chapter 7

Detector Simulations

7.1 Introduction

Chapter 8

Detector Rates

Chapter 9

Physics Simulations

9.1 Introduction

Chapter 10

Estimated Costs and a Rough Schedule

10.1 Introduction

Chapter 11

From fsPHENIX to ePHENIX's Hadron Arm

11.1 Introduction

Acknowledgments

We thank all the colleagues who made comments to the draft of this document, and particularly, thank the following colleagues:

M. Anselmino, R. Vogt.

This work was supported in part by the U.S. Department of Energy, contract numbers xxx.xxx

References

[1] C. Aidala, N. Ajitanand, Y. Akiba, Y. Akiba, R. Akimoto, *et al.*, "sPHENIX: An Upgrade Concept from the PHENIX Collaboration," 2012.

[2] J. Ashman *et al.*, "A measurement of the spin asymmetry and determination of the structure function g1 in deep inelastic muon-proton scattering," *Physics Letters B*, vol. 206, no. 2, pp. 364 – 370, 1988.

[3] R. Jaffe and A. Manohar, "The g1 problem: Deep inelastic electron scattering and the spin of the proton," *Nuclear Physics B*, vol. 337, no. 3, pp. 509 – 546, 1990.

[4] X. Ji, "Gauge-invariant decomposition of nucleon spin," *Phys. Rev. Lett.*, vol. 78, pp. 610–613, Jan 1997.

[5] M. Burkardt, "The Nucleon Spin Sum Rule," 2013.

[6] D. de Florian, R. Sassot, M. Stratmann, and W. Vogelsang, "Global analysis of helicity parton densities and their uncertainties," *Phys. Rev. Lett.*, vol. 101, p. 072001, Aug 2008.

[7] E. Aschenauer, A. Bazilevsky, K. Boyle, K. Eyser, R. Fatemi, *et al.*, "The RHIC Spin Program: Achievements and Future Opportunities," 2013.

[8] G. L. Kane, J. Pumplin, and W. Repko, "Transverse quark polarization in large-p_T reactions, e^+e^- jets, and leptoproduction: A test of quantum chromodynamics," *Phys. Rev. Lett.*, vol. 41, pp. 1689–1692, Dec 1978.

[9] A. Efremov and O. Teryaev, "On Spin Effects in Quantum Chromodynamics," *Sov.J.Nucl.Phys.*, vol. 36, p. 140, 1982.

[10] A. Efremov and O. Teryaev, "QCD Asymmetry and Polarized Hadron Structure Functions," *Phys.Lett.*, vol. B150, p. 383, 1985.

[11] J.-w. Qiu and G. F. Sterman, "Single transverse spin asymmetries," *Phys.Rev.Lett.*, vol. 67, pp. 2264–2267, 1991.

[12] J.-w. Qiu and G. F. Sterman, "Single transverse spin asymmetries in direct photon production," *Nucl.Phys.*, vol. B378, pp. 52–78, 1992.

[13] X.-D. Ji, "Gluon correlations in the transversely polarized nucleon," *Phys.Lett.*, vol. B289, pp. 137–142, 1992.

[14] H. Beppu, Y. Koike, K. Tanaka, and S. Yoshida, "Contribution of Twist-3 Multi-Gluon Correlation Functions to Single Spin Asymmetry in Semi-Inclusive Deep Inelastic Scattering," *Phys.Rev.*, vol. D82, p. 054005, 2010.

[15] F. Yuan and J. Zhou, "Collins Fragmentation and the Single Transverse Spin Asymmetry," *Phys.Rev.Lett.*, vol. 103, p. 052001, 2009.

[16] D. Boer, P. Mulders, and F. Pijlman, "Universality of t-odd effects in single spin and azimuthal asymmetries," *Nuclear Physics B*, vol. 667, no. 12, pp. 201 – 241, 2003.

[17] A. Airapetian *et al.*, "Single-spin asymmetries in semi-inclusive deep-inelastic scattering on a transversely polarized hydrogen target," *Phys. Rev. Lett.*, vol. 94, p. 012002, Jan 2005.

[18] A. Airapetian *et al.*, "Effects of transversity in deep-inelastic scattering by polarized protons," *Physics Letters B*, vol. 693, no. 1, pp. 11 – 16, 2010.

[19] M. Alekseev *et al.*, "Collins and sivers asymmetries for pions and kaons in muon-deuteron dis," *Physics Letters B*, vol. 673, no. 2, pp. 127 – 135, 2009.

[20] M. Alekseev *et al.*, "Measurement of the collins and sivers asymmetries on transversely polarised protons," *Physics Letters B*, vol. 692, no. 4, pp. 240 – 246, 2010.

[21] X. Qian *et al.*, "Single spin asymmetries in charged pion production from semi-inclusive deep inelastic scattering on a transversely polarized ^{3}He target at $Q^2 = 1.4 - 2.7$ gev^2," *Phys. Rev. Lett.*, vol. 107, p. 072003, Aug 2011.

[22] D. Sivers, "Single-spin production asymmetries from the hard scattering of pointlike constituents," *Phys. Rev. D*, vol. 41, pp. 83–90, Jan 1990.

[23] S. J. Brodsky, D. S. Hwang, and I. Schmidt, "Final-state interactions and single-spin asymmetries in semi-inclusive deep inelastic scattering," *Physics Letters B*, vol. 530, no. 14, pp. 99 – 107, 2002.

[24] J. C. Collins, "Leading-twist single-transverse-spin asymmetries: Drellyan and deep-inelastic scattering," *Physics Letters B*, vol. 536, no. 12, pp. 43 – 48, 2002.

[25] Z. Lu and I. Schmidt, "Connection between the sivers function and the anomalous magnetic moment," *Phys. Rev. D*, vol. 75, p. 073008, Apr 2007.

[26] R. D. Klem, J. E. Bowers, H. W. Courant, H. Kagan, M. L. Marshak, E. A. Peterson, K. Ruddick, W. H. Dragoset, and J. B. Roberts, "Measurement of asymmetries of inclusive pion production in proton-proton interactions at 6 and 11.8 gev/ c," *Phys. Rev. Lett.*, vol. 36, pp. 929–931, Apr 1976.

[27] C. E. Allgower *et al.*, "Measurement of analyzing powers of π^+ and π^- produced on a hydrogen and a carbon target with a $22 - \mathrm{GeV}/c$ incident polarized proton beam," *Phys. Rev. D*, vol. 65, p. 092008, May 2002.

[28] D. Adams *et al.*, "Analyzing power in inclusive π^+ and π^- production at high x_f with a 200 gev polarized proton beam," *Phys. Lett. B*, vol. 265, pp. 462–466, 1991.

[29] C. A. Aidala, S. D. Bass, D. Hasch, and G. K. Mallot, "The Spin Structure of the Nucleon," *Rev.Mod.Phys.*, vol. 85, pp. 655–691, 2013.

[30] I. Arsene *et al.*, "Single-transverse-spin asymmetries of identified charged hadrons in polarized *pp* collisions at $\sqrt{s} = 62.4$ GeV," *Phys. Rev. Lett.*, vol. 101, p. 042001, Jul 2008.

[31] B. I. Abelev *et al.*, "Forward neutral-pion transverse single-spin asymmetries in $p + p$ collisions at $\sqrt{s} = 200$ GeV," *Phys. Rev. Lett.*, vol. 101, p. 222001, Nov 2008.

[32] U. D'Alesio and F. Murgia, "Parton intrinsic motion in inclusive particle production: unpolarized cross sections, single spin asymmetries, and the sivers effect," *Phys. Rev. D*, vol. 70, p. 074009, Oct 2004.

[33] C. Kouvaris, J.-W. Qiu, W. Vogelsang, and F. Yuan, "Single transverse-spin asymmetry in high transverse momentum pion production in *pp* collisions," *Phys. Rev. D*, vol. 74, p. 114013, Dec 2006.

[34] J. Koster, "Measurement of Transverse Spin Asymmetries in Polarized proton-proton Collisions, and the Realization of New Electromagnetic Calorimeters for Forward Physics,"

[35] L. Adamczyk *et al.*, "Transverse Single-Spin Asymmetry and Cross-Section for π^0 and η Mesons at Large Feynman-x in Polarized $p+p$ Collisions at $\sqrt{s} = 200$ GeV," *Phys.Rev.*, vol. D86, p. 051101, 2012.

[36] G. Igo, "New STAR transverse spin results," *AIP Conf.Proc.*, vol. 1523, pp. 188–193, 2012.

[37] A. Bravar, D. L. Adams, N. Akchurin, N. I. Belikov, B. E. Bonner, J. Bystricky, M. D. Corcoran, J. D. Cossairt, J. Cranshaw, A. A. Derevschikov, H. En'yo, H. Funahashi, Y. Goto, O. A. Grachov, D. P. Grosnick, D. A. Hill, T. Iijima, K. Imai, Y. Itow, K. Iwatani, K. Krueger, K. Kuroda, M. Laghai, J. L. Langland, F. Lehar, A. de Lesquen, D. Lopiano, F. C. Luehring, T. Maki, S. Makino, A. Masaike, Y. A. Matulenko, A. P. Meschanin, A. Michalowicz, D. H. Miller, K. Miyake, T. Nagamine, F. Nessi-Tedaldi, M. Nessi, C. Nguyen, S. B. Nurushev, Y. Ohashi, Y. Onel, D. I. Patalakha, G. Pauletta, A. Penzo, G. F. Rappazzo, A. L. Read, J. B. Roberts, L. van Rossum, V. L. Rykov, N. Saito, G. Salvato, P. Schiavon, J. Skeens, V. L. Solovyanov, H. Spinka, R. W. Stanek, R. Takashima, F. Takeutchi, D. G. Underwood, A. N. Vasiliev, J. L. White, S. Yamashita, A. Yokosawa, T. Yoshida, and A. Zanetti, "Analyzing power measurement in inclusive λ^0 production with a 200 gev/c polarized proton beam," *Phys. Rev. Lett.*, vol. 75, pp. 3073–3077, Oct 1995.

[38] T. C. Rogers and P. J. Mulders, "No Generalized TMD-Factorization in Hadro-Production of High Transverse Momentum Hadrons," *Phys.Rev.*, vol. D81, p. 094006, 2010.

[39] T. C. Rogers, "Extra Spin Asymmetries From the Breakdown of TMD-Factorization in Hadron-Hadron Collisions," *Phys.Rev.*, vol. D88, p. 014002, 2013.

[40] F. Yuan, "Azimuthal asymmetric distribution of hadrons inside a jet at hadron collider," *Phys.Rev.Lett.*, vol. 100, p. 032003, 2008.

[41] N. Poljak, "STAR results and perspectives on transverse spin asymmetries," *Nuovo Cim.*, vol. C035N2, pp. 193–198, 2012.

[42] R. Fatemi, "Constraining Quark Transversity through Collins Asymmetry Measurements at STAR," *AIP Conf.Proc.*, vol. 1441, pp. 233–237, 2012.

[43] J. C. Collins, S. F. Heppelmann, and G. A. Ladinsky, "Measuring transversity densities in singly polarized hadron-hadron and lepton-hadron collisions," *Nuclear Physics B*, vol. 420, no. 3, pp. 565 – 582, 1994.

[44] R. L. Jaffe, X. Jin, and J. Tang, "Interference fragmentation functions and the nucleon's transversity," *Phys. Rev. Lett.*, vol. 80, pp. 1166–1169, Feb 1998.

[45] A. Vossen *et al.*, "Observation of transverse polarization asymmetries of charged pion pairs in e^+e^- annihilation near $\sqrt{s} = 10.58$ GeV," *Phys. Rev. Lett.*, vol. 107, p. 072004, Aug 2011.

[46] R. Yang, "Transverse Proton Spin Structure at PHENIX," in *American Institute of Physics Conference Series* (M. L. Marshak, ed.), vol. 1182 of *American Institute of Physics Conference Series*, pp. 569–572, Dec. 2009.

[47] A. Airapetian *et al.*, "Evidence for a transverse single-spin asymmetry in leptoproduction of $\pi^+\pi^-$ pairs," *Journal of High Energy Physics*, vol. 2008, no. 06, p. 017, 2008.

[48] H. Wollny, "Transversity Signal in two Hadron Pair Production in COMPASS," 2009.

[49] A. Bacchetta and M. Radici, "Modeling dihadron fragmentation functions," *Phys. Rev. D*, vol. 74, p. 114007, Dec 2006.

[50] A. Bacchetta, F. A. Ceccopieri, A. Mukherjee, and M. Radici, "Asymmetries involving dihadron fragmentation functions: From dis to e^+e^- annihilation," *Phys. Rev. D*, vol. 79, p. 034029, Feb 2009.

[51] L. Bland *et al.*, "Cross Sections and Transverse Single-Spin Asymmetries in Forward Jet Production from Proton Collisions at $\sqrt{s} = 500$ GeV," 2013.

[52] L. Gamberg, Z.-B. Kang, and A. Prokudin, "Indication on the process-dependence of the Sivers effect," *Phys.Rev.Lett.*, vol. 110, p. 232301, 2013.

[53] M. Anselmino, M. Boglione, U. D'Alesio, S. Melis, F. Murgia, *et al.*, "The Sivers effect and the Single Spin Asymmetry A_N in $p^\uparrow p \to hX$ processes," 2013.

[54] C. Adolph *et al.*, "I experimental investigation of transverse spin asymmetries in -p {SIDIS} processes: Collins asymmetries," *Physics Letters B*, vol. 717, no. 45, pp. 376 – 382, 2012.

[55] C. Adolph *et al.*, "{II} experimental investigation of transverse spin asymmetries in -p {SIDIS} processes: Sivers asymmetries," *Physics Letters B*, vol. 717, no. 45, pp. 383 – 389, 2012.

[56] A. Airapetian *et al.*, "Observation of the naive-t-odd sivers effect in deep-inelastic scattering," *Phys. Rev. Lett.*, vol. 103, p. 152002, Oct 2009.

[57] J. P. Ralston and D. E. Soper, "Production of dimuons from high-energy polarized proton proton collisions," *Nucl. Phys.*, vol. B152, p. 109, 1979.

[58] K. Abe *et al.*, "Measurement of azimuthal asymmetries in inclusive production of hadron pairs in e+ e- annihilation at Belle," *Phys. Rev. Lett.*, vol. 96, p. 232002, 2006.

[59] "Measurement of Collins asymmetries in inclusive production of charged pion pairs in e^+e^- annihilation at BABAR," 2013.

[60] M. Anselmino, M. Boglione, U. D'Alesio, A. Kotzinian, F. Murgia, A. Prokudin, and S. Melis, "Update on transversity and collins functions from sidis and data," *Nuclear Physics B - Proceedings Supplements*, vol. 191, no. 0, pp. 98 – 107, 2009. ¡ce:title¿Proceedings of the Ringberg Workshop¡/ce:title¿ ¡ce:subtitle¿New Trends in HERA Physics 2008¡/ce:subtitle¿.

[61] M. Anselmino, M. Boglione, U. D'Alesio, S. Melis, F. Murgia, *et al.*, "Simultaneous extraction of transversity and Collins functions from new SIDIS and e+e- data," *Phys.Rev.*, vol. D87, p. 094019, 2013.

[62] S. J. Brodsky, D. S. Hwang, and I. Schmidt, "Final-state interactions and single-spin asymmetries in semi-inclusive deep inelastic scattering," *Physics Letters B*, vol. 530, no. 1-4, pp. 99 – 107, 2002.

[63] M. Anselmino, M. Boglione, and S. Melis, "A Strategy towards the extraction of the Sivers function with TMD evolution," *Phys.Rev.*, vol. D86, p. 014028, 2012.

[64] A. Bacchetta, A. Courtoy, and M. Radici, "First glances at the transversity parton distribution through dihadron fragmentation functions," *Phys. Rev. Lett.*, vol. 107, p. 012001, Jun 2011.

[65] Z.-B. Kang, J.-W. Qiu, W. Vogelsang, and F. Yuan, "Observation concerning the process dependence of the sivers functions," *Phys. Rev. D*, vol. 83, p. 094001, May 2011.

[66] Danil and Boer, "On a possible node in the sivers and qiusterman functions," *Physics Letters B*, vol. 702, no. 4, pp. 242 – 245, 2011.

[67] R. Field and R. Feynman, "A parametrization of the properties of quark jets," *Nuclear Physics B*, vol. 136, no. 1, pp. 1 – 76, 1978.

[68] D. de Florian, J. Soffer, M. Stratmann, and W. Vogelsang, "Bounds on transverse spin asymmetries for baryon production in pp collisions at {BNL} {RHIC}," *Physics Letters B*, vol. 439, no. 12, pp. 176 – 182, 1998.

[69] N. Brambilla *et al.*, "Heavy quarkonium: progress, puzzles, and opportunities," *Eur. Phys. J. C*, vol. 71, p. 1534, 2011.

[70] R. Vogt, "x_F dependence of ψ' and drell-yan production," *Phys. Rev. C*, vol. 61, p. 035203, 2000.

[71] A. Adare *et al.*, "Cold nuclear matter effects on j/ψ yields as a function of rapidity and nuclear geometry in d+a collisions at $\sqrt{s_{NN}} = 200$ GeV," *Phys. Rev. Lett.*, vol. 107, p. 142301, Sep 2011.

[72] J. L. Nagle, A. D. Frawley, L. A. Linden Levy, and M. G. Wysocki, "Modeling of j/ψ modifications in deuteron-nucleus collisions at high energies," *Phys. Rev. C*, vol. 84, p. 044911, Oct 2011.

[73] K. J. Eskola, H. Paukkunen, and C. A. Salgado, "Eps09 . a new generation of nlo and lo nuclear parton distribution functions," *JHEP*, vol. 04, p. 065, 2009.

[74] K. T. Dmitri Kharzeev, "Signatures of the color glass condensate in j/ψ production off nuclear targets," *Nucl. Phys. A*, vol. 770, p. 40, May 2006.

[75] M. A. Vasiliev *et al.*, "Parton energy loss limits and shadowing in drell-yan dimuon production," *Phys. Rev. Lett.*, vol. 83, pp. 2304–2307, Sep 1999.

[76] S. M. Torbjörn Sjöstrand and P. Skands, "Pythia 6.4 physics and manual," *JHEP*, vol. 05, p. 026, 2006.

[77] J. Pumplin *et al.*, "New generation of parton distributions with uncertainties from global qcd analysis," *JHEP*, vol. 07, p. 012, 2002.

[78] A. Adare *et al.*, "Heavy-quark production in $p + p$ and energy loss and flow of heavy quarks in au + au collisions at $\sqrt{s_{NN}} = 200$ gev," *Phys. Rev. C*, vol. 84, p. 044905, Oct 2011.

[79] A. Adare *et al.*, "Measurement of bottom versus charm as a function of transverse momentum with electron-hadron correlations in $p + p$ collisions at $\sqrt{s} = 200$ GeV," *Phys. Rev. Lett.*, vol. 103, p. 082002, Aug 2009.

[80] L. Adamczyk *et al.*, "Di-electron spectrum at mid-rapidity in $p + p$ collisions at $\sqrt{s} =$ 200 gev," *Phys. Rev. C*, vol. 86, p. 024906, Aug 2012.

[81] H. Agakishiev *et al.*, "High p_T nonphotonic electron production in $p + p$ collisions at $\sqrt{s} = 200$ GeV," *Phys. Rev. D*, vol. 83, p. 052006, Mar 2011.

[82] R. Vogt, "Cold nuclear matter effects on j/ψ and υ production at energies available at the cern large hadron collider (lhc)," *Phys. Rev. C*, vol. 81, p. 044903, Apr 2010.